catalysts

MDPI

Review

Steam Reforming of Bioethanol Using Metallic Catalysts on Zeolitic Supports: An Overview

Francesco Dalena [1], Emanuele Giglio [1,*], Alessia Marino [1], Alfredo Aloise [2], Gianfranco Giorgianni [1], Massimo Migliori [1] and Girolamo Giordano [1]

[1] Chemical Engineering and Catalysis for Sustainable Processes (CECaSP) Laboratory, University of Calabria, Via Pietro Bucci, 87036 Rende, Italy; francesco.dalena@unical.it (F.D.); alessia.marino@unical.it (A.M.); gianfranco.giorgianni@unical.it (G.G.); massimo.migliori@unical.it (M.M.); girolamo.giordano@unical.it (G.G.)

[2] Department of Physical and Chemical Sciences, University of L'Aquila, Via Vetoio (COPPITO 1–2), 67100 L'Aquila, Italy; alfredo.aloise@univaq.it

* Correspondence: emanuele.giglio@unical.it

Abstract: Hydrogen is considered one of the energy carriers of the future due to its high mass-based calorific value. Hydrogen combustion generates only water, and it can be used directly as a fuel for electricity/heat generation. Nowadays, about 95% of the hydrogen is produced via conversion of fossil fuels. One of the future challenges is to find processes based on a renewable source to produce hydrogen in a sustainable way. Bioethanol is a promising candidate, since it can be obtained from the fermentation of biomasses, and easily converted into hydrogen via steam catalytic reforming. The correct design of catalysts and catalytic supports plays a crucial role in the optimization of this reaction. The best results have to date been achieved by noble metals, but their high costs make them unsuitable for industrial application. Very satisfactory results have also been achieved by using nickel and cobalt as active metals. Furthermore, it has been found that the support physical and chemical properties strongly affect the catalytic performance. In this review, zeolitic materials used for the ethanol steam reforming reaction are overviewed. We discuss thermodynamics, reaction mechanisms and the role of active metal, as well as the main noble and non-noble active compounds involved in ethanol steam reforming reaction. Finally, an overview of the zeolitic supports reported in the literature that can be profitably used to produce hydrogen through ethanol steam reforming is presented.

Keywords: bioethanol; steam reforming; hydrogen; zeolite

Citation: Dalena, F.; Giglio, E.; Marino, A.; Aloise, A.; Giorgianni, G.; Migliori, M.; Giordano, G. Steam Reforming of Bioethanol Using Metallic Catalysts on Zeolitic Supports: An Overview. *Catalysts* **2022**, *12*, 617. https://doi.org/10.3390/catal12060617

Academic Editor: Rosalinda Mazzei

Received: 4 May 2022
Accepted: 1 June 2022
Published: 3 June 2022

1. Introduction

Nowadays, the development of environmentally friendly fuels is considered one of the greatest technological challenges. The energy dependence on fossil fuels is considered one of the main threats both to world economic development (in particular of those countries that are not energy-independent) and to the protection of the planet's environment.

Indeed, global warming and climate change are pushing scientific research to develop alternative fuels, environmentally friendly and renewable, with increased energy density [1,2]. Among the investigated alternatives, with their overall carbon neutrality, biofuels are considered valuable components in the energy mix of modern economies [3,4]. The first- and second-generation of biofuels are used in direct combustion processes (primary biofuels), whilst secondary biofuels can be obtained by thermochemical (combustion, pyrolysis and gasification) [5], chemical or biological conversion of residual, waste or side products [6]. Examples of the biofuels and sustainable energy sources are bio-oils, char, pellets [7], and biodiesel from lignocellulosic biomass [8]; green diesel and jet fuels from microalgae oils [9,10]; sugar-derived ethanol [11] and H_2 [12]; 2-methylfuran from fur-

fural [13–16]; H_2 from municipal solid waste [17]; dimethyl ether from syngas (via biomass gasification) or CO_2 hydrogenation and methanol dehydration [18–24].

Among the various chemicals from biomass, ethanol (EtOH) certainly plays a crucial role for its versatility, relative low production costs, availability and low toxicity [12,25,26]; it is also promising for the sustainable production of useful compounds, such as hydrocarbons/olefins [27–29] and hydrogen via aqueous phase [30] or ethanol steam reforming (ESR) [31–33].

Due to its high mass-based heating value (120 MJ/kg), hydrogen is considered a promising energy carrier since its combustion generates only water without any greenhouse gas emission. Hydrogen can be directly employed as fuel for electricity production and for automotive applications [34–36]. Furthermore, H_2 can be used for ammonia synthesis [37] or in combination with CO and CO_2 to produce synthetic fuels and chemicals, such as methane [38,39], methanol [40], and hydrocarbon mixtures [41]. Nowadays, more than 90% of worldwide hydrogen production comes from fossil fuels, but this molecule can be used for the chemical storage of intermittent renewable energy sources via water electrolysis [42,43].

In the overall reaction of the ESR, 1 mol of EtOH and 3 mol of water produce 6 mol of hydrogen in a strongly exothermic reaction [44–47]:

$$C_2H_5OH + 3H_2O \rightarrow 2CO_2 + 6H_2 \qquad \Delta H_r{}^{\circ}{}_{298K} = 174 \text{ kJ mol}^{-1} \quad (1)$$

Research interest in catalytic ESR increased in the last two decades [48]. To maximize hydrogen production, it is crucial to work with an excess of steam, also minimizing the ethanol dehydration (EDHy) and decomposition. Coke formation and metal sintering are the main problems for the stable operation of catalytic ESR. Coke formation is mainly due to the Boudouard reaction, oligomerization of ethylene or decomposition of methane formed during ESR. Coke can considerably reduce the catalyst activity, affecting the catalyst structure and occupying the catalytic sites [48,49].

Depending on the catalyst type and support, the ESR mechanism may follow different pathways as several other reactions may occur, affecting the overall H_2 yield. Such a complex reaction pathway requires the tailoring of proper catalysts and support to address the reaction toward hydrogen production with a maximum yield and selectivity [50].

Various materials have been proposed to increase catalyst activity and stability: supported metals, such as rhodium (Rh), nickel (Ni) and cobalt (Co), have attracted attention as efficient catalysts at relatively low temperatures (300–400 °C) [51–56].

The use of economic materials for the catalytic system is desired form the perspective of sustainable industrial applications. Zeolites are effective microporous catalysts that can be used as support in ESR, due to their morphological properties (well-defined crystalline structure, high specific surface areas, uniform pores and good thermal stability) [57]. When using zeolites in metal catalyzed reactions, one of the main scientific challenges is the catalyst stability as the acid sites of zeolitic supports can favor ethanol dehydration instead of dehydrogenation with the consequent formation of ethylene that tends to form coke [58]. In turn, coke could deposit on the surface of the catalyst, affecting its performance and leading to progressive deactivation. Therefore, adequate strategies for limiting the formation of coke are the control of acidity and the improvement of the metal dispersion in order to reduce the sintering. Zeolite support can be used for the deposition of small Ni particles, but in presence of significant acidity (due to heteroatoms insertion in the framework, such as Al), it might favor coke formation, especially at low temperatures [59]. To overcome those difficulties, different techniques can be used to reduce the zeolite acidity (for example, post-synthesis dealumination) [60–62], also promoting the formation of small metal particles and reducing coke formation as a consequence [33]. In addition, the metal–support interaction strength could be tuned: a greater dispersion of the metal also prevents metal sintering under the operating conditions for ESR [63].

With respect to previous general reviews in the field [12,32,33,64], this paper proposes the systematic analysis of zeolite-based catalysts for ESR, mostly prepared using base metals

as redox sites, highlighting the most important catalyst design features. Accordingly, in the first part, the thermodynamics of the process and potential reaction mechanisms occurring on metallic active sites are briefly discussed. Then, the mainly used active metals for the ESR are discussed, especially focusing on non-noble ones that can potentially improve its economic feasibility. Finally, the main zeolite-based catalysts in the open literature are discussed in relation to their potential profitability for H_2 production.

2. Ethanol Steam Reforming

2.1. Thermodynamics of Ethanol Steam Reforming

In this section, the thermodynamics of hydrogen production via ESR is considered. The effect of reaction temperature and pressure on the outlet gas composition is investigated. As reported in Equation (1), ESR can be ideally expressed by means of a single reaction leading to the production of hydrogen and carbon dioxide.

The chemical equilibrium composition was calculated through the minimization of Gibbs free energy for a stoichiometric reaction mixture. Figure 1a presents the equilibrium gas composition at 1.5 bar for a temperature range between 200 and 800 °C, while Figure 1b presents the hydrogen yield as a function of temperature for different pressure values, calculated according to the following equation:

$$\eta_{H_2} = \frac{\dot{n}_{H_2}}{6 \cdot \dot{n}_{C_2H_5OH}} \quad (2)$$

where coefficient 6 represents the stoichiometric coefficient ratio between hydrogen and EtOH in Equation (1).

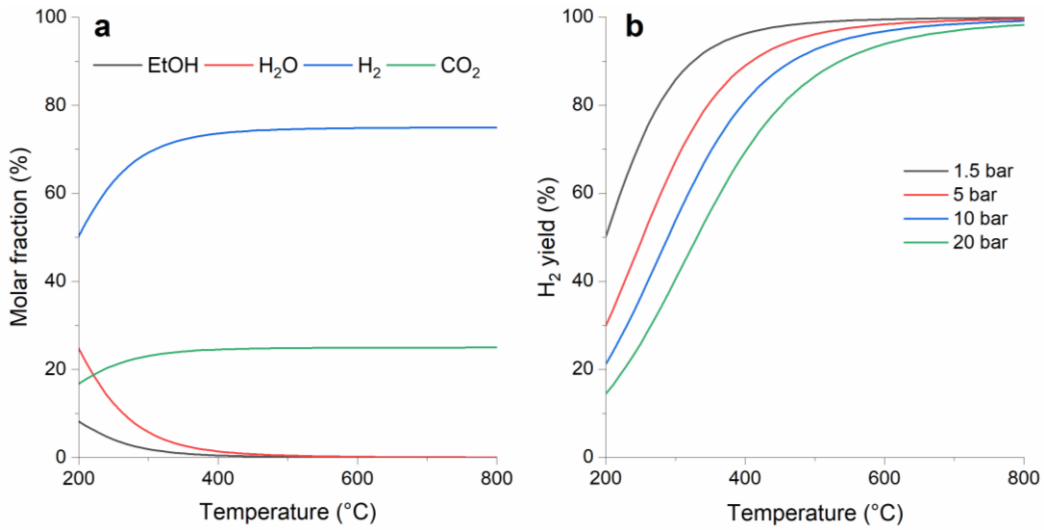

Figure 1. ESR equilibrium composition, considering only the components in reaction (1): (**a**) effect of temperature on equilibrium mixture at 1.5 bar and (**b**) thermodynamic hydrogen fractional yield at different temperatures and pressures. The equilibrium was calculated via Gibbs free energy minimization.

As expected, temperature increase favors hydrogen formation because the investigated reaction is endothermal. A plateau in the hydrogen yield is already reached at ≈400 °C, if the reaction of Equation (1) is carried out at 1.5 bar. As suggested by thermodynamics and as shown in Figure 1b, high pressure limits hydrogen yield since reaction (1) proceeds with an increase in the mole number.

In real operating conditions, the reaction pathway of ESR includes three reactions: ethanol dehydrogenation (EDH) (3), acetaldehyde steam reforming (ASR) (4) and water gas shift reaction (WGS) (5) [33].

$$C_2H_5OH \leftrightarrow CH_3CHO + H_2 \qquad \Delta H_r{}^{\circ}{}_{298K} = 68.9 \text{ kJ mol}^{-1} \quad (3)$$

$$CH_3CHO + H_2O \leftrightarrow 2CO + 3H_2 \qquad \Delta H_r{}^\circ{}_{298K} = 168.8 \text{ kJ mol}^{-1} \quad (4)$$

$$CO + H_2O \leftrightarrow CO_2 + H_2 \qquad \Delta H_r{}^\circ{}_{298K} = -41.4 \text{ kJ mol}^{-1} \quad (5)$$

At low temperatures, exothermic WGS is thermodynamically favored but CO for water gas shift should be produced from reaction (4), which is, in turn, endothermal and thus favored at high temperatures, as well as reaction (3). Increasing the reaction temperature should thus favor hydrogen production, but a maximum in H_2 yield/selectivity may occur. Various undesired side reactions may take place in ESR reaction conditions, such as ethanol dehydration into ethylene (6), the decomposition of acetaldehyde (7) and acetone formation (8). Furthermore, aldol condensation and coke formation are also reported [33].

$$C_2H_5OH \leftrightarrow C_2H_4 + H_2O \qquad \Delta H_r{}^\circ{}_{298K} = 45.5 \text{ kJ mol}^{-1} \quad (6)$$

$$CH_3CHO \leftrightarrow CH_4 + CO \qquad \Delta H_r{}^\circ{}_{298K} = -19.3 \text{ kJ mol}^{-1} \quad (7)$$

$$CH_3CHO \leftrightarrow CH_3COCH_3 + CO + H_2 \qquad \Delta H_r{}^\circ{}_{298K} = 4.1 \text{ kJ mol}^{-1} \quad (8)$$

Particularly, acetaldehyde decomposition is targeted for its suppression because it produces inactive methane, decreasing the hydrogen selectivity as consequence. The promotion of adsorbed acetate species formation from acetaldehyde is effective for the preferential promotion of the ASR and the suppression of the acetaldehyde decomposition to CH_4. The methanation of CO (9) and CO_2 (10) are hydrogen-consuming undesired reactions that should be inhibited as much as possible during ethanol steam reforming [33]. Furthermore, reactions (9) and (10) are undesirable since they are very exothermal reactions (see reaction enthalpy values) and it is very difficult to control the reactor temperature when these reactions take place. From a thermodynamic and kinetic standpoint, a temperature rise is not challenging, but it may compromise the catalyst integrity.

$$CO + 3H_2 \leftrightarrow CH_4 + H_2O \qquad \Delta H_r{}^\circ{}_{298K} = -206.1 \text{ kJ mol}^{-1} \quad (9)$$

$$CO_2 + 4H_2 \leftrightarrow CH_4 + 2H_2O \qquad \Delta H_r{}^\circ{}_{298K} = -164.8 \text{ kJ mol}^{-1} \quad (10)$$

These additional reactions introduce new compounds among the possible equilibrium products. Thus, the equilibrium calculation was carried out via global Gibbs energy minimization also assuming the presence of methane, acetaldehyde, acetone and carbon monoxide.

Figure 2 presents the simulation results revealing that ethylene, acetone and acetaldehyde are present only in traces when equilibrium is reached. Especially at low temperatures, methane formation is thermodynamically favored over the hydrogen one. This is mainly due to the equilibrium of the methanation reaction, leading to high conversion at temperatures below 400 °C. This behavior is amplified when pressure increases since methanation reactions (9) and (10) undergo through a mole reduction. On the other hand, H_2 molar fraction grows with increasing temperature because its production is favored by the thermodynamics of the ESR reaction (1). At 1.5 bar, the hydrogen yield presents a peak at ≈700 °C, as hydrogen production is counterbalanced by the consumption via reverse water gas shift (RWGS), which is endothermal and starts to be predominant at high temperatures. This trend is confirmed by the simultaneous increase in CO and decrease in CO_2 molar fractions when the temperature rises (especially above 600 °C).

Even though some reactions are favored by thermodynamics, the situation may thus change in the presence of a catalyst enabling only some reaction routes and affecting reaction kinetics. An ideal catalyst should inhibit methanation reaction, especially if the target consists of ESR at low temperatures. Furthermore, such catalyst should not enable (as preferential reaction routes) ethanol dehydration (EDHy) to ethylene, as well as all the reaction steps leading to carbon formation and deposition.

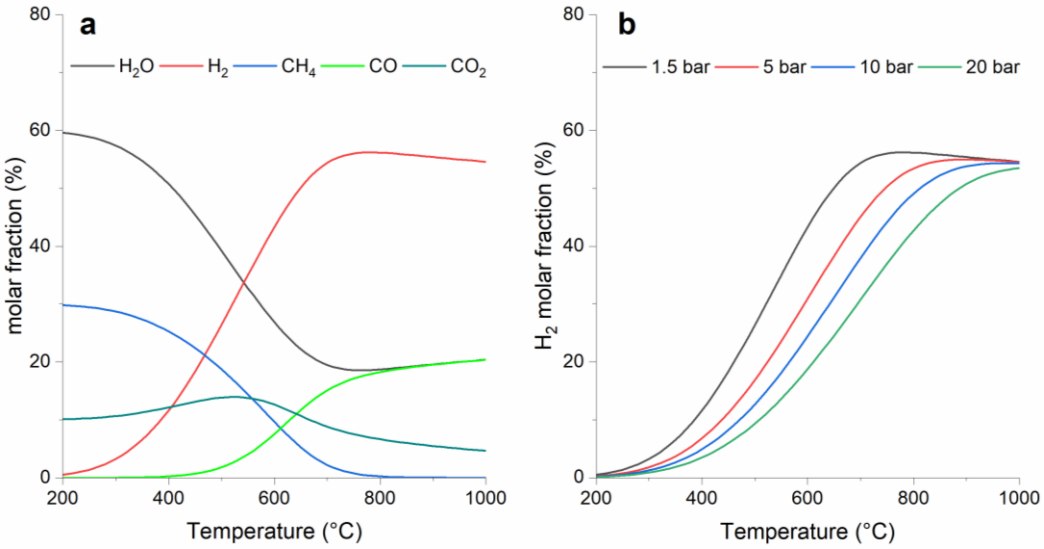

Figure 2. ESR equilibrium with stoichiometric inlet mixture: (**a**) effect of temperature on outlet composition at 1.5 bar and (**b**) H_2 outlet molar fraction vs. temperature at different pressures. The equilibrium was calculated via Gibbs free energy minimization.

Several coke-forming reactions may also occur in ESR, via ethylene (11) or methane decomposition (12) and Boudouard reaction (13). Suppressing ethylene and methane formation and promoting WGS reaction can thus limit carbon deposition [33].

The addition of excess steam can be a solution for carbon formation as it is usually limited by increasing the steam excess. This aspect is offset by consequences on energy efficiency due to the required heat for generating steam, which should be considered during the whole process energy (and economic) analysis.

$$C_2H_4 \leftrightarrow C_{(s)} + 2H_2 \qquad \Delta H_r^{\circ}{}_{298K} = -52.3 \text{ kJ mol}^{-1} \tag{11}$$

$$CH_4 \leftrightarrow C_{(s)} + 2H_2 \qquad \Delta H_r^{\circ}{}_{298K} = -74.9 \text{ kJ mol}^{-1} \tag{12}$$

$$2CO \leftrightarrow C_{(s)} + CO_2 \qquad \Delta H_r^{\circ}{}_{298K} = -172.6 \text{ kJ mol}^{-1} \tag{13}$$

Sharma et al. [31] reviewed the phenomenon of carbon formation during ESR, including the effect of involved active metal, support and operating conditions. Furthermore, the main strategies to limit the catalyst deactivation due to coking were summarized. The authors pointed out as the best approach to reduce catalyst deactivation due to carbon formation is either by preventing carbon from forming or, if formed, by converting it into the gaseous species for easy removal [31]. Some aspects related to the relationship between active metals and carbon formation are briefly mentioned in the following sections.

2.2. Reaction Mechanism

Figure 3 summarizes plausible reaction pathways involved in the ESR over the metal surface, based on both experimental and theoretical results. The EtOH activation may occur via several pathways. One possibility is the cleavage of O–H bond, followed by a dehydrogenation forming intermediates such as acetaldehyde (CH_3CHO^*), acetyl (CH_3C^*O), ketene ($^*CH_2C^*O$) and ketenyl ($^*CHC^*O$). Another possible pathway is represented by the C–H bond activation and a subsequent dehydrogenation, preserving the O–H bond with the formation of generic intermediates of the type $^*CH_yCH_x{}^*OH$. Finally, the cleavage of bonds O–H and C–H may occur, forming the intermediate $^*CH_2CH_2O^*$ (oxametallacycle). These pathways can take place simultaneously, depending on the nature of the metal. The cleavage of the C–C bond within the chemisorbed intermediates can be followed by the hydrogenation/dehydrogenation of CH_x^*, water activation and the oxidation of C* species [65,66].

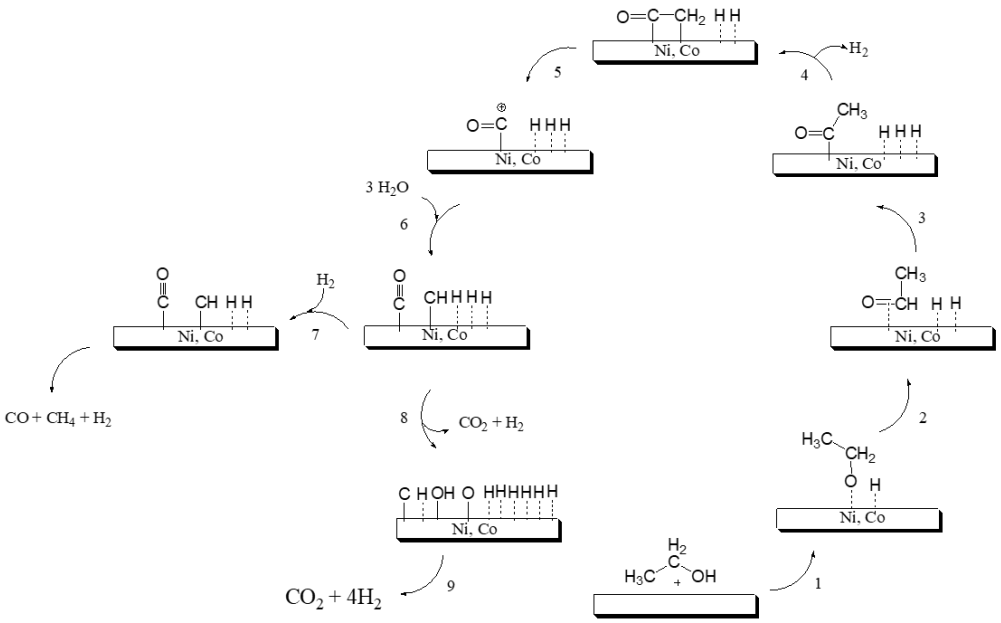

Figure 3. ESR reaction pathways as a function of temperature for metals such as nickel and cobalt (adapted from [65]).

The oxidation of C* is crucial in ESR in order to prevent catalyst deactivation via carbon formation. The development of catalysts for ESR is related to the tuning of different stages: ethanol activation, C* formation and the removal of the C*, as well as the ability to inhibit the hydrogenation rearrangements of CH_x fragments leading to methane formation at low temperatures [65].

EtOH activation usually occurs through its O–H group. Nevertheless, recent studies have shown that ethanol can be activated through C–H bonds [67]. EtOH activation is an important step in determining the main reaction pathway. Dehydrogenated intermediates will bring interesting information to elucidate the C–C bond cleavage, usually occurring in an intermediate with a high dehydrogenation level.

For all pathways, CH_4 selectivity is affected by the ability of the metal to hydrogenate/dehydrogenate the CH_x* species [68]. Methane formation at low temperatures is undesirable because the reforming of CH_4 (leading to hydrogen production) will only occur at greater temperatures (typically above 800 °C). The activation of H_2O is of paramount importance in ESR due to the role of *OH species in oxidation steps. After the C–C bond cleavage and steam activation, the CO adsorbed on the metal is oxidized to generate CO_2 via water gas shift (WGS) [65]. CH_x species oxidation on the metal proceeds at about 320 °C. The most widely accepted mechanism for the oxidation of CH_x species is CH_x decomposition to C*, followed by oxidation to CO [65].

In summary, there are still some open questions related to the reaction mechanism of ESR on different metals. The right balance of the involved steps is crucial for the catalyst performance optimization, as well as for the sample stability against carbon deposition [65].

3. Metals for ESR

Several active metals have been recently investigated for ESR, including both noble (Rh, Ru, Pd, Ir and Pt) and non-noble metals (Ni and Co), generally active in the range 300–500 °C [69]. The activity decreases in the order of Rh > Co > Ni > Pd, consistent with their resistance to coke formation [34,70].

Although noble metal catalysts afford high ESR activity, their industrial application is mainly limited by the high cost [71,72]. Therefore, such metals will not be further discussed in this paper.

Co and Ni-based catalysts present lower activity than noble metals for the ESR reaction. Moreover, deactivation by coking, sintering and methane formation (e.g., via hydrogenation

of CO and CO_2) limit their potential [33,73]. However, even in the presence of the reported drawbacks, their low costs make them attractive for ESR. Moreover, redox supports and promoters, such as CeOx or MnOx, mitigate their deactivation by coking [74,75].

Among the non-noble metals, nickel shows the highest methane formation [33]. However, this metal is still widely used for ESR due to its significant bond-braking (e.g., C–C, O–H and C–H) [33,69] and H_2 recombination capability. As previously shown, Ni dehydrogenates EtOH to hydrogen and acetaldehyde [65] at low temperatures. Besides, the C–C bond cleavage also occurs when increasing temperatures, leading to acetaldehyde decomposition into methane, carbon monoxide and hydrogen. Therefore, due to the C–C bond-breaking activity, the decomposition of ethanol (14) and acetaldehyde conversion to methane and CO easily proceed over Ni catalysts. Then, the Methane Steam Reforming (MSR) (15) and WGS reaction (5) lead to H_2 and CO_2. Notably, the endothermal MSR is not thermodynamically favored at low temperatures, leading to increased CH_4 selectivity [33].

$$C_2H_5OH \rightarrow CH_4 + CO + H_2 \qquad \Delta H_r{}^{\circ}{}_{298K} = 49.6 \text{ kJ mol}^{-1} \tag{14}$$

$$CH_4 + 2H_2O \rightarrow CO + 3H_2 \qquad \Delta H_r{}^{\circ}{}_{298K} = 206.1 \text{ kJ mol}^{-1} \tag{15}$$

For this reason, conventional nickel-based catalysts generally produce a greater number of byproducts (coke and CH_4) than cobalt-based ones.

On the other side, highly dispersed Ni on hierarchical BEA zeolites present low deactivation by coking due to the low driving force for carbon diffusion [69]. Similarly, improved coking and sintering resistance were found on Ni/perovskites. Moreover, Sharma et al. [31] evidenced how highly dispersed metallic particles favor the oxidizing activity, while larger metallic particles promote carbon formation because of a reduced interaction with the support. It emerges that the preparation of highly dispersed Ni catalysts is advantageous from several points of view. Therefore, the sol–gel method [69,76] and the deposition of Ni on microporous/mesoporous supports are highly advantageous for preparing durable catalysts, promoting the presence of highly dispersed Ni particles [69] and increasing the catalyst activity as a consequence. Several studies focused on the dependence of the catalytic activity on the controlled size of metal particles [77]. Specifically, higher activities were observed using particles with average diameters lower than 5 nm due to their greater surface energy [78]. Notably, besides the presence of highly dispersed and stable metals, supports also play a key role in activity due to their acidity/basicity and interaction with the active phase (metal–support interaction) [31]. Specifically, basic supports could inhibit ethanol dehydration (EDHy) to ethylene, thus limiting one of the precursors for carbon formation [33]. Among the investigated supports were Al_2O_3, SiO_2, CeO_2, La_2O_3, ZrO_2 [75,79–83], promoted M-Al_2O_3 (M = La, Zr, Ti), Ce-SiO_2, [33], zeolites (BEA, ZSM-5, and Y) [33,69,84–86] and mesoporous materials (SBA-15, MCM-41) [54,87,88].

Cobalt, similarly to Ni, seems to favor the formation of acetaldehyde at low temperatures [65], enabling the formation of carbon oxides and decreasing their methane formation activity [33]. DFT studies [33] have shown that metallic Co favors C–C cleavage, while Co^{2+} species enable water activation and acetate species formation. Notably, while metallic Co is also active for coke formation, Co^{2+} can oxidize the deposited coke, enabling the formation of activated OH_x species. Therefore, the control of Co^0/Co^{2+} ratio is crucial to prevent catalyst deactivation [49]. Conversely, other species, such as Co_3O_4 spinel formed in the case of Co/CeO_2 catalysts, together with metallic Co and CoO, are inactive [33,64,89].

Ni-Co bimetallic catalysts have shown a higher activity than single Ni or Co catalysts [54,87,90,91]. The idea is to exploit the positive characteristics of both metals in a synergistic way: nickel showed great activity, especially in the C–C cleavage, while cobalt usually limits coke formation. Furthermore, cobalt addition can promote WGS reaction [33].

The typical performances of the recently reported Ni, Co, and Ni–CO catalysts are reported in Table 1. A wider results overview can be found in previous reviews [33,64]. Notably, the space velocities reported in Table 1 were calculated in different ways: by referring to the whole inlet flow, the EtOH mass flow, the reaction volume or the catalyst

mass. In some works [53–55,87,92], space velocity was calculated as the ratio between total inlet flow (mL h^{-1}) and catalyst load (in grams). When total inlet flow (i.e., reacting mixture plus inert gas) is considered, reacting mixture mole concentration (or, in other terms, dilution grade) also plays a role, as the reaction rate is proportional to the reactants' partial pressure.

Table 1. Recent ESR studies on nickel, cobalt and bimetallic Ni-Co catalysts: operating condition, EtOH conversion and hydrogen yield.

Catalyst	Steam-to-Carbon Ratio (S/C)	T (°C)	Space Velocity	Ethanol Conversion	H_2 Yield	Ref.
Ni/SiO_2	3	500	W/F_{EtOH} = 91.88 g_{cat} s $g_{EtOH}{}^{-1}$	≈35%	≈20%	[46]
Ni/Al_2O_3-La_2O_3	3	450	23,140 mL h^{-1} $g_{cat}{}^{-1}$	100%	62%	[83]
10 Ni/TiO_2-Al_2O_3	1.5	500	WHSV = 2773 h^{-1}	93%	75%	[93]
$10Ni/CeO_2$	6	420	60,000 mL $g_{cat}{}^{-1}$ h^{-1}	100%	68%	[94]
10Ni/SBA-15	1.85	500	60,000 mL $g_{cat}{}^{-1}$ h^{-1}	69%	41%	[87]
17Co/α-Al_2O_3	3	500	GHSV= 51700 h^{-1}	86%	64%	[95]
$29Co/CeO_2$	6	500	60,000 mL $g_{cat}{}^{-1}$ h^{-1}	100%	94%	[53]
$29Co/CeO_2$	3	500	60,000 mL $g_{cat}{}^{-1}$ h^{-1}	≈85%	≈80%	[53]
10Co-0.3Ce/SEP (Sepiolite)	3	600	WHSV = 21.5 h^{-1}	91%	69%	[96]
10Co/SEP (Sepiolite)	3	600	WHSV = 21.5 h^{-1}	54%	34%	[96]
10Co/SBA-15	1.85	500	60,000 mL $g_{cat}{}^{-1}$ h^{-1}	89%	49%	[92]
$10Co/Al_2O_3$	1.5	550	72,000 mL $g_{cat}{}^{-1}$ h^{-1}	99%	86%	[55]
9Ni-1Co/MCM-41	2.5	490	9000 mL $g_{cat}{}^{-1}$ h^{-1}	90%	80%	[54]
5Ni-5Co/MCM-41	2.5	490	9000 mL $g_{cat}{}^{-1}$ h^{-1}	≈80%	≈65%	[54]
1Ni-9Co/MCM-41	2.5	490	9000 mL $g_{cat}{}^{-1}$ h^{-1}	≈75%	≈60%	[54]
(Ni, Co) NPs (Nanoparticles) (Ni/Co = 0.26)	3	500	GHSV = 324,000 h^{-1}	100%	87%	[90]
8Ni-2Co/SBA-15	1.85	500	60,000 mL $g_{cat}{}^{-1}$ h^{-1}	86%	53%	[87]
5Ni-5Co/SBA-15	1.85	500	60,000 mL $g_{cat}{}^{-1}$ h^{-1}	68%	43%	[87]
2Ni-8Co/SBA-15	1.85	500	60,000 mL $g_{cat}{}^{-1}$ h^{-1}	59%	42%	[87]
20Ni-20Co/CeO_2	3	500	W/F => 0.12 g_{cat} h $mol_{EtOH}{}^{-1}$	≈85%	≈55%	[91]

A comparison between different catalysts should take into account all the parameters affecting the operating conditions: temperature, space velocity, inert presence and steam-to-carbon ratio (EtOH conversion will be higher if a steam-excess inlet mixture is employed). Furthermore, the catalyst should be usually activated/reduced by flowing hydrogen (pure or diluted) at high temperatures before activity testing in order to reduce the metal oxide presence.

By rationalizing main findings, nickel and cobalt can be employed as non-noble active metals for ESR. Bimetallic Ni-Co-based catalysts are extremely promising, as they can synergistically combine the advantages of both the main non-noble metals employed for ESR. Furthermore, in previous research works, it has been pointed out that catalysts with reduced metal particle sizes are more active and stable [33,97,98]. Besides the metal particles' size, metal oxidation state control can help (especially when cobalt is employed) in limiting carbon formation.

Catalyst performance (activity and stability) is strongly affected by the support in terms of the metal–support interaction and acidity/basicity: acid supports can drive the formation of ethylene, which is considered a precursor for coke formation.

4. Zeolitic Support for ESR

Besides the selection of metal phases, the support plays a major role in catalytic reactions. A high surface area and the heat resistance of the support can improve the catalytic activity and stability [31].

Large surface area supports, such in the case of γ-Al_2O_3 [99–101], mesoporous silica materials [88,102,103] and mixed oxides [104,105], usually allow for the formation of strongly dispersed surface precursors and retard sintering processes. Zeolites possess remarkable properties, such as well-defined crystalline structures, good thermal stability, high internal surface area, intracrystalline mesopores [106] and low potential for support–metal interactions; such properties make this class of materials suitable for use as catalyst support [107].

Their channel structure enables the flow of EtOH molecules into the channel (generically, the diameter of the microporous structure of the zeolite utilized as support is slightly bigger than that of EtOH), while extending the time of reaction and promoting the EtOH reaction on active sites. Hierarchical zeolites have highly ordered transgranular and intragranular mesopore channels, large surface area, pore volume and thick pore walls [69].

Zeolite and mesoporous materials are very interesting materials not only for acid-catalyzed reactions, but also promoting red–ox reactions since it is very easy to incorporate some metals in the zeolitic framework or to add metals by the ionic exchange procedure [108,109].

As discussed above, the EtOH molecules in the stream reforming reaction are dehydrogenated, leading to the formation of ethoxy groups. A mechanism that favors this reaction is the absorption of EtOH on the surface of the catalysts. Such species can be subsequently transformed into various intermediates by successive EDH and EDHy reactions, C–C bond scission and oxidative surface reactions with the contribution of hydroxyl groups or oxygen species in the catalysts [85].

However, the acidity of the zeolites could also enhance the cracking and isomerization of the formed hydrocarbon (Figure 4) [110]. For this reason, the high molar concentration of the acid sites present on the surface of the zeolite support can catalyze the reaction toward the formation of undesired by-products [85].

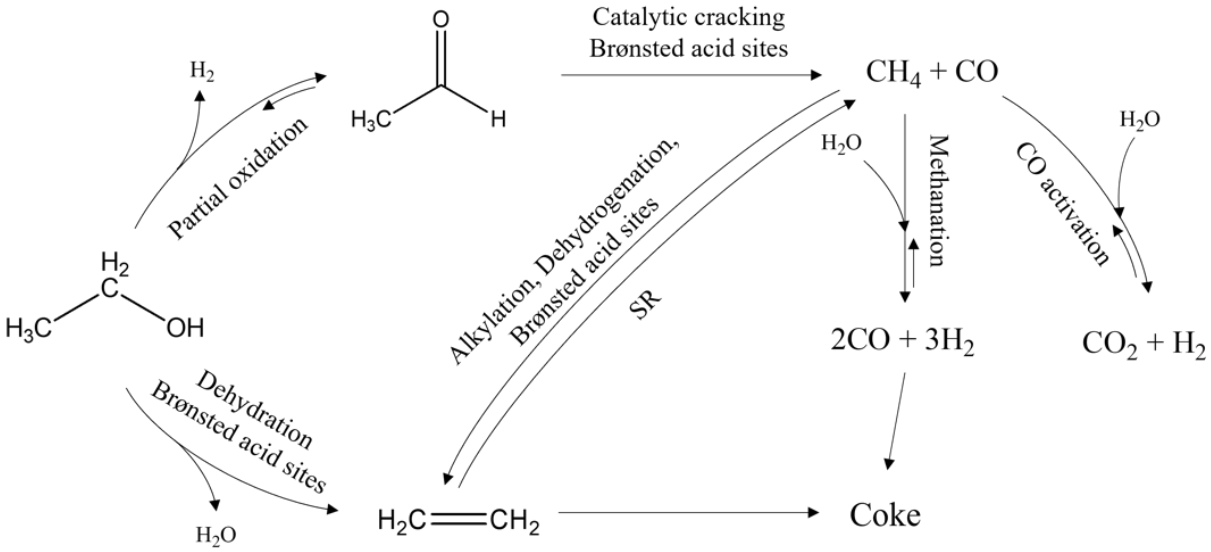

Figure 4. Reactions involved in the ethanol steam reforming and influence of the acid sites (adapted from [64]).

The building blocks of the zeolite are SiO_4 tetrahedra (with trivalent Al^{3+} cation substituting Si^{4+}) [111]. The angle formed by atoms varies in a broad interval (130–180°) [112], giving rise to the elevated number of known zeolite structures [110]. The introduction of trivalent aluminum atoms in the tetrahedral framework brings negative charges, balanced by extra-framework cations [113]. Protons acting as compensating cations near aluminum centers behave as Brønsted acid sites [23,27,114–118], while tri-coordinated silicon atoms located on small structure defects act as electron-acceptor sites, i.e., as Lewis acid centers [113].

It has been mentioned that the acidity of the support is not a determining parameter during the ESR reaction at high temperatures, while a minimum concentration of the Brønsted sites is sufficient to promote the EDHy into ethylene and consequently the coke formation even at low temperatures [59,119,120]. Moreover, different zeolites have been investigated as catalytic support in ESR.

4.1. ZSM-5 Zeolites

ZSM-5 is a high-silica zeolite widely used as catalyst and its applicability in ESR and was investigated [56,121]. The framework type of the high-silica zeolite ZSM-5 can be described in terms of units, but it is easier to use pentasil units. These units are linked to form pentasil chains, and mirror images of these chains are connected via oxygen bridges to form corrugated sheets with 10-member ring holes. Each sheet is linked by oxygen bridges to the next to form the 3-dimensional structure. Adjacent sheets are related to one another by an inversion center. This produces straight 10-member ring channels parallel to the corrugations (along y) and sinusoidal 10-member ring channels perpendicular to the sheets (along x). Both channel types are interconnected to one another, forming a 3D 10-member ring channel system. Because the pores are formed of 10-member rings rather than 12-member rings, the shape selectivity for sorption and catalysis is different from that of FAU- or EMT-type zeolites, and this fact determined different catalytic applications as ZSM-5 is used in different refinery and petrochemical processes [122].

The physical characteristics of this zeolite make it good from a dimensional point of view if applied as a catalytic support for the ESR reaction [59]. Furthermore, the structure of the interconnected channel of the ZSM-5 zeolite can limit the deactivation of the catalyst caused by coke when ESR is carried out at high temperatures [57].

Kumar et al. [50] have tested ZSM-5 zeolite (with Si/Al ratio equal to 50) coupled with non-noble metals (Ni and Co). Prepared via wet impregnation, samples were subsequently tested at a space velocity of 35.4 g_{gas} h^{-1} $g_{cat}{}^{-1}$. The performance of ZSM-5 has shown a more than 90% EtOH conversion at 450 °C. However, the product distribution varied with the temperature and the active metals deposited. The 10 wt.-% Ni/ZSM-5 catalyst has shown higher C_2H_4 and lower H_2 selectivity than the 10 wt.-% Co/ZSM-5 samples, indicating that Ni is more active for the scission of the C–C bond at low temperatures with ZSM-5 support as compared to Co.

Lang et al. [56] tested metal/zeolite catalytic structures prepared with Rh and ZSM-5 treated with an alkaline solution. The use of the alkaline solution has the dual objective of exchanging cations of alkali metals (to reduce the intrinsic acidity of the zeolite) and to induce a mesoporosity via zeolite desilication. They found that the introduction of secondary porosity allows the better diffusion of reactants delaying the micropores blocking. The different diffusive flow rate lowered the deposition of carbon in the micropores, significantly improving the catalyst stability since an induced secondary mesoporosity reduces the diffusion limitation. The best results were obtained by treating a ZSM-5 with a solution of K_2CO_3 [56]. The authors reported that modified support improves the Rh dispersion preventing sintering as the metal was deposited via the wet impregnation method using a solution of $RhCl_3$, allowing a concentration of 1% (w/w) of the metal in the final structure of the catalyst. From the characterization data, it can be deduced that the treatment led both to the insertion of K as counter-ion (about 3 wt.-%) and to suitable modifications of the support structure. Changes occurred mainly in terms of Si/Al ratio reduction (from 80 to 48.1) and textural properties (see Table 2). The ion exchange led to a significant decrease in acid sites from 450 mmol g^{-1} (for zeolite in H-form) to 93.5 mmol g^{-1} for modified ZSM-5. The net drop in acidity allows the catalytic system to work even at low temperatures; EtOH conversion (X) at 300 °C and at 400 °C was reported to be equal to 79.27% and 99.07%, respectively. H_2, CO and C_2H_4 selectivity (S) are reported in Table 2. The authors justify this as a synergic effect between the active Rh component and the structure of the zeolite, which reduces the selectivity of CO produced via RWGS down to less than 3.5% at 400 °C. At low temperatures, the main reactions are the EDH to

acetaldehyde (3) and its subsequent decarboxylation to CH_4 and CO. The ASR and MSR reactions are not easy to be conducted at low temperatures, resulting in high CH_4 selectivity for all catalysts with promising hydrogen selectivity [56].

Table 2. ZSM-5 and MOR support for various types of metal catalysts for the ESR reaction.

Metal	Support				Experimental Condition		X_{EtOH} (%)	Selectivity (%)					Ref.
	Type	*Si/Al*	S_{BET} ($m^2 \cdot g^{-1}$)	V_{micro} ($cm^3 \cdot g^{-1}$)	*T* (°C)	*Space Velocity*		H_2	*CO*	CO_2	CH_4	C_2H_4	
Co (10 wt.-%)	ZSM-5	50	440	0.281	500 600	WHSV = 35.4 g_{gas} h^{-1} g_{cat}^{-1}	~97 ~100	~45 ~60	~1 ~40	~1 ~20	~8 ~6	~90 ~25	[50]
Ni (10 wt.-%)	ZSM-5	50	345.5	0.190	500 600		~97 ~100	~47 ~72	~5 ~20	~16 ~24	~13 ~10	~43 ~0	
Rh (1 wt.-%)	ZSM-5	48.1	*305*	0.083	300 400	n.a.	79 ~100	28 33	29 3	18 47	48 46	2 1	[56]
Ni (19.9 wt.-%)	MOR	10	360	0.18	400	GHSV = 4700 h^{-1}	84.3	24.1	1.6	5.8	2.8	64.2	[123]
Ni (19.4 wt.-%)	MOR (treated)	10	340	0.06	400	GHSV = 4700 h^{-1}	97.5	69.0	8.2	4.4	14.4	0.6	

Conversion and selectivity data of Ref. [50] were extrapolated from the graph.

Similar investigations were performed on MOR-type zeolites [123]. Additionally, in this case, the zeolite was desilicated (with a 0.2 M NaOH solution) to generate mesoporosity and to reduce the acid sites. The catalyst, including Ni based on desilicated MOR zeolite, showed a high activity, selectivity and resistance to coke deposition. Catalytic tests were carried out with a large steam excess in the inlet mixture (H_2O/EtOH = 13). The results suggest that the mesoporosity generated in this MOR-type zeolite makes the Ni–MOR catalytic system even more selective towards hydrogen at relatively low temperatures (400 °C).

4.2. BETA Zeolites

The structure of zeolite beta is found to be a high defective intergrowth of two distinct new zeolite frameworks, named polymorphous A and B, respectively [124]. Zeolite beta compositions, thus, represent a narrow window of a broader family of zeolites, of which the polymorph A and B structures with unfaulted staking sequences represent the two end members. All members of this family of zeolites have two sets of perpendicular channels, which intersect to form a three-dimensional array of cages that have three 12-member ring apertures [125]. Zeolite beta is disordered in the c-direction. That is, well-defined layers are stacked in a random way. The units are joined to one another via four rings to form layers with saddle-shaped 12-member rings. Adjacent layers are related to one another by a rotation of 90° [126].

The disorder arises because this rotation can be in either a clockwise or counter-clockwise sense. If the counter-clockwise or clockwise rotation was maintained throughout the crystal, the structure would be ordered and chiral. Interestingly, whatever the stacking sequence, a 3-dimensional 12-member ring channel system results; so, for catalytic applications, the stacking sequence is not important [122]. The average diameter of the microporous structure of the BEA zeolite is intrinsically larger (6.7 Å) than that of the ZSM-5-type (from 5.1–5.6 Å). This characteristic allows the better diffusion of ethanol [29,59,69]. As in the case of ZSM-5, if the catalytic system works at low temperatures (300–500 °C), the Bronsted acid sites of the zeolite catalyze the EDHy reaction with a consequent high yield of ethylene. For example, a Ni-BEA catalyst (Ni: 10 wt.-%) tested at 500 °C tends to rapidly deactivate (decreasing values of conversion, of *S* to H_2 and CO_2 selectivity, and increasing values of ethylene selectivity), despite having excellent values of EtOH conversion and H_2 selectivity in the first hours of the reaction as reported from Gac et al. [85]. To minimize the production of ethylene, the authors reported on the testing of tested dealuminated BEA zeolite as support. The removal of aluminum atoms from the zeolite structure not only led to a drastic acidity reduction (Bronsted acid sites decreased from 268 to 3 μmol g^{-1},

while Lewis acid sites decreased from 130 to 3 μmol g^{-1} after dealumination), but also led to a slight decrease in crystallinity, which promoted the stabilization of the metal nanoparticles. BEA dealumination favored the adsorption of Ni precursors, hindering the agglomeration of the ionic species of the metal [59,127]. This catalytic material showed a greater active surface area than the non-dealuminated one. The sample was tested at 500 °C for 20 h and showed the complete conversion of the EtOH [85]. In the first hour of the reaction, the catalytic system of the non-dealuminated beta led to a higher hydrogen yield than that of the dealuminated zeolite (85% against 76%). However, the hydrogen selectivity for the unmodified zeolite drastically decreased (about 60%) in the first 5 h of time on stream (TOS) for the benefit of the ethylene yield (about 60% after three hours of reaction). This means that this kind of catalyst was more effective in olefin formation. Dealuminated zeolite, instead, showed a good constant H_2 selectivity during all the 20 h of the reaction and also showed ethylene yield (Y) values close to 0 for about 17 h of the reaction. Despite the excellent results, the problems that arose for these catalysts is that the produced CO during ESR from the dealuminated sample was higher than that generated in the non-modified sample.

In several applications, H_2 must be extremely pure, and the admitted percentage of impurities must be extremely low. For example, if hydrogen is used for PEM fuel cell applications, the acceptable content of CO is 10 ppm [128–130]. For this reason, the catalytic performance of the Ni-BEA catalyst was also studied by introducing other metals to maximize the yield of H_2 and CO_2, by converting the undesired by-products. In the work of Tian et al. [131], the acid force of the zeolite support is limited by partially replacing the Al content with trivalent Fe cations in the structure, thus limiting the concentration of proton sites within the catalyst. This hetero-atom substitution is very easy, as demonstrated in different articles [132,133]. In addition, the introduction of metals with variable valence inside the zeolite structure can improve the chemical–physical properties by satisfying the needs of specific catalytic reactions [131]. The Fe introduced in the structure has a different bond length (the Fe–O bond is 0.197 nm, while the Al–O bond is 0.175 nm), leading to a partial distortion of the crystal lattice. This Fe–BEA-type zeolitic support reduced the order of the mesoporous phase and led to a decrease in the number of both moderate and strong acid sites. Such a decrease in acid sites inhibited the EDHy, while the presence of Fe improved the yield of the WGS reaction. In particular, the 10% Ni/0.15% Fe–BEA catalyst showed an H_2 selectivity of up to 72.15% and an EtOH conversion rate of 99.6% at 500 °C, while the amount of coke deposition was 4.3% after a 12 h reaction [131].

Using a trimetallic system with Cu, Fe, and Ni (loaded with 1.5, 1.5, and 10 wt.-%, respectively), a greater catalytic activity was found compared to monometallic catalysts, especially at low temperatures (300 ° C). Zheng et al. [134] showed how the synergistic effect among the Ni, Cu, and Fe phases influences the different reaction pathways. Figure 5 shows the reaction scheme as a function of the catalytic activity of the specific metals.

The first reaction step is the formation of acetaldehyde through the EDH catalyzed by the Cu sites. At 300 °C, Ni is active in the transformation of acetaldehyde into CH_4 and CO, since, at this temperature, there is almost exclusively this reaction as the C–C bond strength of EtOH is much higher than that of acetaldehyde [72]. Cu has not completed its catalytic activity; in fact, at temperatures of 300 °C, it is strongly active in the transfection of CO (formed by EDHy) into H_2 and CO_2 through the WGS reaction. At temperatures above 350 °C, Fe catalyzes the ASR reaction, while at temperatures above 450 °C, it catalyzes the MSR reaction. From these experimental results, it is evident that the Fe and Cu phases play an important role in the ESR reaction mechanism, especially at low temperatures as promoters. The synergy of the Ni, Cu and Fe phases maintained the activity of the catalyst almost constant for 28 h [72].

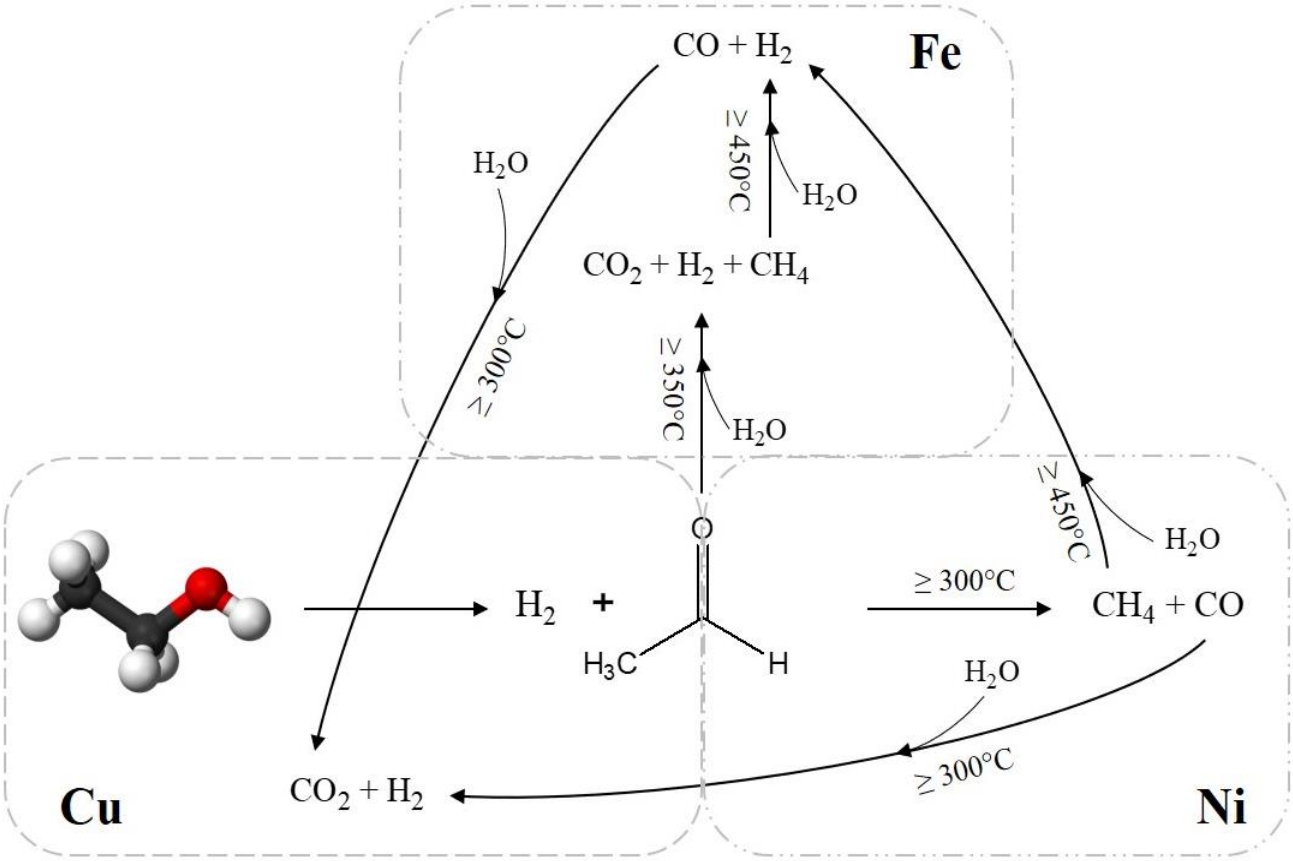

Figure 5. Schematic reaction pathway of the ESR reaction over the Cu/Fe/Ni_BEA system (adapted from [72]).

Table 3 presents the results of experimental investigations carried out over BEA-supported metal catalysts.

Table 3. BEA support for various types of metal catalysts for the ESR reaction.

Metal	Support				Experimental Condition		X_{EtOH} (%)	Selectivity (%)					Ref.
	Type	Si/Al	S_{BET} (m^2 g^{-1})	V_{micro} (cm^3 g^{-1})	T (°C)	Space Velocity		H_2	CO	CO_2	CH_4	C_2H_4	
Ni (10 wt.-%)	BEA	17	481.7	0.48	500	WHSV ≈ 9.5 g_{EtOH} h^{-1} g_{cat}^{-1}	100	60	3	30	1	70	[85]
Ni (10 wt.-%)	BEA		496.8	0.42	500		100	75	10	55	35	0	
Ni (10 wt.-%)	BEA	100	570	0.19	300 400 500	WHSV ≈ 7.35 g_{EtOH} h^{-1} g_{cat}^{-1}	≈87 ≈97 100	≈35 ≈57 ≈68	≈14 ≈7 ≈5	≈9 ≈17 ≈20	≈16 ≈11 ≈7	n.a. n.a. n.a.	[72]
Fe (1.5 wt.-%) Cu (1.5 wt.-%) Ni (10 wt.-%)	BEA	100	508	0.21	300	WHSV ≈ 7.35 g_{EtOH} h^{-1} g_{cat}^{-1}	≈90	≈52	≈7	≈15	≈14	n.a.	
					400		≈99	≈68	≈3	≈21	≈8	n.a.	
					500		100	≈72	≈3	≈21	≈4	n.a.	

Conversion and selectivity data of Ref. [72] were extrapolated from the graph.

4.3. Y Zeolite

Zeolite Y is another type of zeolite suitable for industrial applications also because of its affordable cost [135], especially for the catalyst used in fluid catalytic cracking processes. Zeolites Y have different forms: NaY zeolite synthesized from sodium aluminosilicate gels, NH^{4+} and HY zeolites prepared from zeolite Y by ion exchange with NH_4Cl or polyvalent metal cations followed by the thermal treatment [136,137], and Ultra Stable Y (USY) zeolite

characterized from a bulk Si/Al ratio higher than the Y form, resulting from hydrothermal treatments [138]. The cubic unit cell of all these aluminosilicates contains 192 (Si,Al)O_4 tetrahedrons [126].

Inokawa et al. [139] tested nickel supported over zeolite Y in ESR. The first results showed that the incorporation of transition metal cations in the Y-type zeolite structure using an ion exchange process has a significant influence on ESR (Table 4). In fact, this type of catalytic support led to the production of C_2H_4 mainly during reforming with EtOH steam, indicating that the presence of cations favored the EDHy. A second study by the same authors on the type of catalysts [140] showed how basicity controlled by the exchange of alkaline cations in a zeolite (exchange of Na with K and Cs) led to a change in the characteristics of both the support and metal. Improved reducibility and catalytic activity led to a higher H_2 yield and selectivity. Hydrogen selectivity has been related with the size of the cation (Ni/Na_Y < Ni/K_Y < Ni/Cs_Y). As previously shown, the dehydrogenation reaction of EtOH was accelerated by the basicity of the zeolite, while the EDHy was inhibited. The addition of K in catalysts using Y-type support was also investigated on Rh/NaY samples. Potassium addition favored the conversion of EtOH, which increased from 62 to 97% [84]. The authors of this study concluded that the addition of K increased the yield of hydrogen, but the flow of reactants has a greater influence. In fact, the results show that, at the same temperature (300 °C) and H_2O/EtOH molar ratio (5:1) and with the same catalyst (K-Rh/NaY), there is a marked increase in the selectivity of hydrogen, which passes from about 45% for a reagent flow equal to 2.04 g min^{-1} to about 68% for a reagent flow equal to 2.77 g min^{-1}. It has also been [141] shown that catalysts of the Mg/Ni/Ga_Y tend to reduce the formation of coke on the catalyst compared to the bimetallic catalyst Ni/Mg_Y. This type of catalyst showed a very high selectivity of H_2 and CH_4 only at a temperature ranging from 550 °C to 750 °C. Additionally, in this case, the results show how the multi-metal component plays a different role to that of the ESR reaction by increasing the EtOH conversion and H_2 yield to 100% and 87%, respectively (see Table 4). This high performance was maintained for up to 59 h at a temperature of 700 °C (H_2O/EtOH = 3 and GHSV = 6740 h^{-1}).

Table 4. Y-type zeolite-supported catalysts for ESR.

Metal	Support		Experimental Condition		Product/Ethanol Feed					Ref.
	Type	Si/Al	T (°C)	Space Velocity	H_2	CO	CO_2	CH_4	C_2H_4	
Ni (9 wt.-%)	Na_Y	2.75	300	96.8	3.8	0.4	0.1	0.2	0.06	[140]
	K_Y	2.75	300	96.8	4.7	0.5	0.2	0.4	0.01	
	Cs_Y	2.75	300	96.8	5.7	0.7	0.2	0.5	0.01	
Ni (4.5 wt.-%)	Y (Ni loaded via wet impregnation)	2.75	300	8	7.0	0.9	0.5	0.5	0.2	[139]
Ni (2.4 wt.-%)	Y (Ni loaded via ionic exchange)	2.75	300	8	0.5	0.0	0.0	0.0	29.5	

4.4. ITQ Zeolites

Pure silica ITQ-2 [142] and ITQ-18 [143] are two zeolites with a high external surface area that have shown good results as catalytic supports for Ni and Co metals for ESR. These catalytic systems have shown excellent performances in terms of catalytic activity, H_2 selectivity and low coke deposition. The excellent catalytic properties can be related to the low molar concentrations of acid sites in the zeolite. In fact, the absence of acid sites in pure silica ITQ zeolites limits the EDHy reaction that leads to the formation of ethylene and consequently of coke. Low coke deposition can be correlated with both the high external surface and the structure with a series of external pockets distributed along

of sheets, which favor the stabilization of Ni and Co metal, improve their dispersion and prevent their agglomeration.

When the ITQ-2-supported catalysts are tested above 500 °C, H_2, CO_2, CO and CH_4 are the only products. Both the catalysts Co_ITQ-2 and Ni _ITQ-2 exhibit lower CO selectivity and high hydrogen yields (see Table 5). The total absence of acid sites strongly limits the production of ethylene and, consequently also, the catalyst deactivation; both samples remain active even after 72 h at a temperature of 400 °C [142].

Table 5. ITQ-18 and ITQ-2 support for Co and Ni catalysts for the ESR reaction.

Catalyst	Support			Experimental Condition		X_{EtOH} (%)	Selectivity (%)					Ref.
	Type	S_{BET} ($m^2 \cdot g^{-1}$)	*Pore Volume (BJH)* ($cm^3 \cdot g^{-1}$)	*T* (°C)	*Space Velocity*		H_2	*CO*	CO_2	CH_4	C_2H_4	
Co (19.9 wt.-%)	ITQ-18	293	0.17	500 °C	GHSV ≈ 4700 h^{-1}	97.9	71.2	3.1	19.5	5.7	0.1	[143]
Co (20.1 wt.-%)	ITQ-2	507	0.54	300 °C 400 °C 500 °C	GHSV ≈ 4700 h^{-1}	≈70 ≈86 ≈97	≈55 ≈62 ≈69	≈12 ≈4 ≈1	≈8 ≈15 ≈21	~15 ~16 ~9	≈0 ≈0 ≈0	[142]
Ni (19.5 wt.-%)	ITQ-2	517	0.53	300 °C 400 °C 500 °C	GHSV ≈ 4700 h^{-1}	≈77 ≈95 ≈100	≈50 ≈59 ≈66	≈18 ≈12 ≈2	≈2 ≈10 ≈21	~19 ~18 ~10	≈0 ≈0 ≈0	

Conversion and selectivity data of Ref. [142] were extrapolated from graphs.

In the case of Co_ ITQ-18 catalysts [143], after 24 h of activity, no deactivation was detected, even though there was a significant concentration of deposited coke correlated to the slightly acidic properties of the ITQ-18 zeolite (Si/Al = 100). The catalytic system Co_ITQ-18 (H_2O/EtOH = 13, GHSV = 4700 h^{-1}, atmospheric pressure and temperature equal to 500 °C), showed high values of both H_2 selectivity (71% after 24 h), but it also produced very low concentrations of CO and CH_4 (of 3.1% and 5.7%, respectively).

4.5. Core Shell Zeolites

As seen before, the use of Ni deposited on zeolite support tends to greatly improve the catalytic activity and the H_2 yield, especially at low temperatures. However, the competitive catalytic effects of the various metals lead to the excessive production of by-products, such as CO, CH_4, and acetaldehyde. Therefore, a further challenge for the ESR reaction is the control of by-product formation and, thus, the selective production of hydrogen.

Core-shell type nanoparticles can be defined as constituted by a core (inner material) and a shell (outer layer material) [144,145]. These types of materials combine the advantages of the passivation induced by the shell with the high surface area and accessible pore channels of the core, offering new opportunities in several applications [146,147]. Furthermore, the successful synthesis of several zeolite composites, such as MFI-MEL, MFI-MFI, BEA-MFI and MOR-MFI, with core–shell structures for different catalytic areas has been reported [148,149]. In the specific case of the ESR reaction, the core–shell metal zeolitic structures showed both a great catalytic activity and a high selectivity of H_2 even at low temperatures, as well as properties in the reduction of by-products [148,150–152].

Very promising results have been obtained using a BEA-type zeolite structure as a shell surrounding a metal core [148,152] (Table 6). Various research works propose the synthesis of a metallic nucleus for the reaction of ESR dispersed over different supports. A variety of products, such as H_2, CO_2, CH_4, CO and intermediate acetaldehyde, are obtained within the core structure [151].

Table 6. Core–shell support for the various types of metal catalysts for the ESR reaction.

Core		Shell		Support		Experimental Condition		X_{EtOH} (%)	Selectivity (%)				Ref.
Metal	*Type*	*Metal*	*Type*	S_{BET} ($m^2 \cdot g^{-1}$)	V_{TOT} ($cm^3 \cdot g^{-1}$)	*T* (°C)	*WHSV* (g_{EtOH} h^{-1} g_{cat}^{-1})		H_2	*CO*	CO_2	CH_4	
Pt (1 wt.-%) (core + shell)	BEA	Pt (1 wt.-%) (core + shell)	SiO_2	557	0.65	300 350 400	8.5	≈98 ≈100 ≈100	≈64 ≈68 ≈72	≈4 ≈2 ≈1	≈19 ≈21 ≈22	≈10 ≈7 ≈2	[151]
Cu (2.5 wt.-%) Fe (2.5 wt.-%)	BEA	Ni (10 wt.-%)	Al-BEA	428	0.24	300 350 400	7.3	≈97 ≈100 ≈100	≈57 ≈69 ≈67	≈4 ≈0 ≈2	≈21 ≈24 ≈28	≈18 ≈7 ≈2	[152]
Ni (22 wt.-%) (core + shell)	BEA	Ni (22 wt.-%) (core + shell)	BEA	295.5	1.19	350 400 450 500	29.4	≈85 ≈89 ≈92 ≈95	≈76 ≈73 ≈72 ≈71	≈7 ≈6 ≈8 ≈8	≈16 ≈18 ≈17 ≈17	≈1 ≈3 ≈2 ≈2	[153]

Conversion and selectivity values were extrapolated from graphs.

The products then pass through the shell again. A schematic representation of the diffusion in core–shell zeolites is represented in Figure 6.

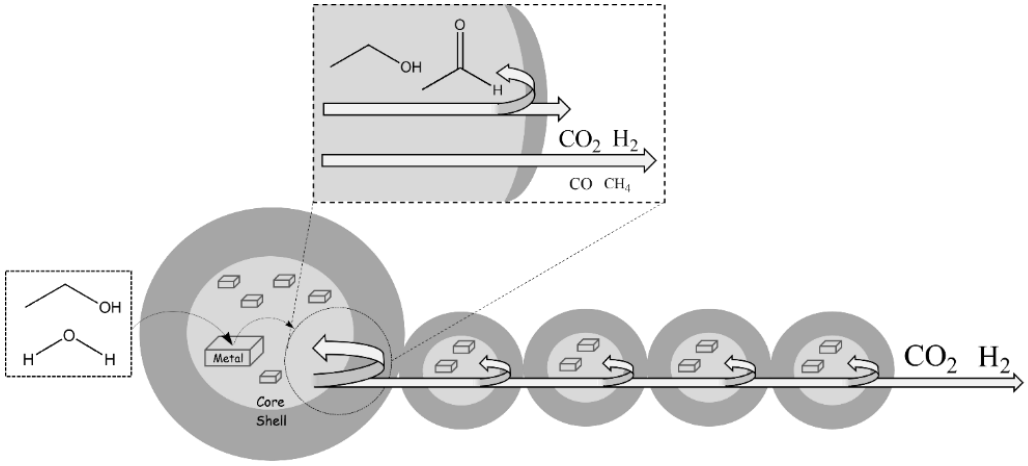

Figure 6. Schematic representation of the ESR reaction over the core–shell system (adapted from [151]).

The addition of some metals within the catalytic system can favor the transformation of by-products into CO_2 and H_2. For example, as seen previously, the addition of Cu inside the catalytic system can considerably improve the ability to break the O–H bond even at low temperatures, thus favoring both a complete conversion of EtOH and the MSR reaction, while the addition of Fe tends to catalyze the reaction of ASR and WGS [153]. The mixture of gaseous by-products, such as CO and CH_4, therefore tends to pass through core–shell systems positioned in series. The catalytic activity of the metals favoring MSR and WGS enables the syngas purification from the smaller molecular size by-products within these systems. Zheng et al. [152] studied BEA-type core–shell catalysts consisting of a core supporting Cu and Fe and a Ni-based shell. The results showed significantly improved catalytic activity and a better H_2 selectivity if compared to the BEA-type zeolite as support. Furthermore, the presence of Cu and Fe contributed to obtain high purity syngas.

5. Comparison and Future Trend

The previous paragraphs show that the ESR reaction is a reliable alternative to obtain "green" hydrogen, especially when using biomass-derived ethanol. However, a rationally designed catalysts and optimized conditions are necessary to maximize H_2 yields and minimize its environmental impact (e.g., decreasing the amounts of GHG by-products

such as CO, CO_2 and CH_4) (Table 2–6). Al_2O_3 was considered as suitable supports for this reaction due to its favorable textural properties and thermal stability. Since then, several non-noble metals/supports have been reported.

A comparison of the most promising catalysts, although unfair (due to the very different conditions reported in the literature), is reported in Table 7. Among these, metal-loaded zeolite (e.g., Ni/dealuminated BEA) and core–shell zeolite catalysts (with different distributions of one or more metals within the core and the shell zeolites of the composite particles) led to promising hydrogen yields and decreased formation of by-products and coke, even at low temperatures (Table 7). In particular, the catalyst developed by Wang et al. [153] demonstrated a high H_2 selectivity, low coke formation and high stability (>100 h TOS).

Table 7. Comparison of ESR catalytic performance among various catalytic systems.

Sample Name	Operating Conditions				X_{EtOH} (%)	S_{H2} (%)	Ref.
	Temperature (°C)	*Space Velocity*	*EtOH/H_2O*	*TOS* (h)			
Pt-CeO_2@Ni-SiO_2	400	WHSV = 8.9 h^{-1}	1:6	28	100	~67	[154]
Co-Ni/_La-Ce	550	WHSV = 2.26 h^{-1}	1:6	60	90 (100% for the first 20 h)	~69	[155]
Co/CeO_2_N-CA (Citric Acid)	420	GHSV = 60,000 mL g^{-1} h^{-1}	1:12	21	~60	~76	[75]
Pt-Cu@Ni-SiO_2	450	WHSV = 7.2 h^{-1}	1:6	50	100	~71	[156]
Ni(10)/Ga(30)/Mg(30)_Zeolite Y	600	WHSV = 6.7 h^{-1}	1:3	59	100	~69	[141]
Ni_{10}SiBEA	500	WHSV = 9.5 g_{EtOH} $h^{-1}g_{cat}{}^{-1}$	1:12	22	100	~65 (~75 for t = 18 h)	[85]
10.0 wt% Co_xO_y@Pd_ Zeolite Y	600	GHSV = 16,800 h^{-1}	1:3	45	100	75–100	[150]
2.5Fe2.5CuSB@NB (Si-Beta core and Ni-Beta shell)	500	WHSV = 7.3 h^{-1}	1:6	8	100	71	[152]
NiNPs/OH-MBEA	400	WHSV = 29.4 h^{-1}	1:5	100	~93	~77	[153]

6. Conclusions

The present work reviewed the thermodynamics and most suitable catalysts for hydrogen production via a low-temperature ethanol steam reforming reaction, focusing on the hybrid catalyst using zeolites as supports.

As compared with noble metals, nickel and cobalt ensure a good trade-off between costs and performance in the perspective of an economically feasible process. However, catalyst deactivation by coking is still an issue. Moreover, as suggested by the thermodynamic analysis, methane formation should be minimized to maximize the hydrogen yield. Therefore, active metals with decreased methane formation ability are ideally required. The addition of synergistic active metals to the main active metal, e.g., Ni added with Fe and Cu, promotes the water gas shift, acetaldehyde steam reforming and methane steam reforming, maximizing the yield of hydrogen and CO_2. Compared to other supports, zeolites, due to their microporous features, allow the preparation of highly dispersed metallic phases. However, the presence of Bronsted acid sites can also lead to olefin formation and coking as a consequence. On the contrary, using alkali metal-doped zeolites as support coking can be effectively avoided also maximizing the H_2 yields. At the same time, among the reviewed zeolites, the 12-member-ring pore system of the BEA zeolite is ideal for the ethanol steam reforming reaction due to its peculiar structure and texture. Further improvements can be achieved using dealuminated BEA (drastically reducing the amount of Bronsted acid sites) and core–shell particles with different distributions of active metals in the core and shell zeolites.

Author Contributions: Conceptualization, F.D. and A.A.; methodology, F.D. and E.G.; software, E.G. and A.M.; formal analysis, F.D., E.G. and G.G. (Gianfranco Giorgianni); resources, F.D. and G.G. (Girolamo Giordano); data curation, F.D. and E.G.; writing—original draft preparation, F.D., E.G. and G.G. (Girolamo Giordano); writing—review and editing; F.D., G.G. (Gianfranco Giorgianni) and M.M; visualization, E.G. and A.M.; supervision A.A., M.M. and G.G. (Girolamo Giordano). All authors have read and agreed to the published version of the manuscript.

Funding: This research received no external funding.

Conflicts of Interest: The authors declare no conflict of interest.

List of Abbreviations

ASR	acetaldehyde steam reforming
EDH	ethanol dehydrogenation
EDHy	ethanol dehydration
ESR	ethanol steam reforming
EtOH	ethanol
GHSV	gas hourly space velocity
MSR	methane steam reforming
$\dot{n}$	mole flow (mol s^{-1})
PEM	polymer electrolyte membrane
S	selectivity of a reaction product
S_{BET}	specific surface area (m^2 g^{-1})
T	temperature (°C)
TOS	time on stream (h)
V_{micro}	volume of micropores (cm^3 g^{-1})
WGS	water gas shift reaction
WHSV	weight hourly space velocity
X	conversion of the limiting reactant
Y	product yield
$\Delta H_r{}^{\circ}{}_{298K}$	reaction enthalpy at standard condition (kJ mol^{-1})
η	product yield

References

1. Sayed, E.T.; Wilberforce, T.; Elsaid, K.; Rabaia, M.K.H.; Abdelkareem, M.A.; Chae, K.; Olabi, A.G. A Critical Review on Environmental Impacts of Renewable Energy Systems and Mitigation Strategies: Wind, Hydro, Biomass and Geothermal. *Sci. Total Environ.* **2021**, *766*, 144505. [CrossRef]
2. Wasif, M.; Shahbaz, M.; Sinha, A.; Sengupta, T.; Qin, Q. How Renewable Energy Consumption Contribute to Environmental Quality? The Role of Education in OECD Countries. *J. Clean. Prod.* **2020**, *268*, 122149. [CrossRef]
3. Dalena, F.; Senatore, A.; Iulianelli, A.; Di Paola, L.; Basile, M.; Basile, A. Ethanol from Biomass: Future and Perspectives. In *Ethanol: Science and Engineering*; Elsevier Inc.: Amsterdam, The Netherlands, 2018; pp. 25–59.
4. Rajeswari, S.; Baskaran, D.; Saravanan, P.; Rajasimman, M.; Rajamohan, N.; Vasseghian, Y. Production of Ethanol from Biomass–Recent Research, Scientometric Review and Future Perspectives. *Fuel* **2022**, *317*, 123448. [CrossRef]
5. Molino, A.; Migliori, M.; Macrì, D.; Valerio, V.; Villone, A.; Nanna, F.; Iovane, P.; Marino, T. Glucose Gasification in Super-Critical Water Conditions for Both Syngas Production and Green Chemicals with a Continuous Process. *Renew. Energy* **2016**, *91*, 451–455. [CrossRef]
6. Dalena, F.; Senatore, A.; Basile, M.; Marino, D.; Basile, A. From Sugars to Ethanol—From Agricultural Wastes to Algal Sources: An Overview. In *Second and Third Generation of Feedstocks: The Evolution of Biofuels*; Elsevier Inc.: Amsterdam, The Netherlands, 2019; pp. 3–34, ISBN 9780128151624.
7. Yu, Y.; Wu, J.; Ren, X.; Lau, A.; Rezaei, H.; Takada, M.; Bi, X.; Sokhansanj, S. Steam Explosion of Lignocellulosic Biomass for Multiple Advanced Bioenergy Processes: A Review. *Renew. Sustain. Energy Rev.* **2022**, *154*, 111871. [CrossRef]
8. Kumar, D.; Singh, B.; Korstad, J. Utilization of Lignocellulosic Biomass by Oleaginous Yeast and Bacteria for Production of Biodiesel and Renewable Diesel. *Renew. Sustain. Energy Rev.* **2017**, *73*, 654–671. [CrossRef]
9. Papanikolaou, G.; Lanzafame, P.; Giorgianni, G.; Abate, S.; Perathoner, S.; Centi, G. Highly Selective Bifunctional Ni Zeo-Type Catalysts for Hydroprocessing of Methyl Palmitate to Green Diesel. *Catal. Today* **2020**, *345*, 14–21. [CrossRef]
10. Hoang, A.T.; Sirohi, R.; Pandey, A.; Nižetić, S.; Lam, S.S.; Chen, W.-H.; Luque, R.; Thomas, S.; Arıcı, M.; Pham, V.V. Biofuel Production from Microalgae: Challenges and Chances. *Phytochem. Rev.* **2022**, 0123456789. [CrossRef]
11. Dalena, F.; Senatore, A.; Iulianelli, A.; Di Paola, L.; Basile, M.; Basile, A. Ethanol From Biomass. In *Ethanol*; Elsevier: Amsterdam, The Netherlands, 2019; pp. 25–59, ISBN 9780128114582.
12. Sanchez, N.; Ruiz, R.; Hacker, V.; Cobo, M. Impact of Bioethanol Impurities on Steam Reforming for Hydrogen Production: A Review. *Int. J. Hydrogen Energy* **2020**, *45*, 11923–11942. [CrossRef]
13. Giorgianni, G.; Abate, S.; Centi, G.; Perathoner, S.; van Beuzekom, S.; Soo-Tang, S.-H.; Van der Waal, J.C. Effect of the Solvent in Enhancing the Selectivity to Furan Derivatives in the Catalytic Hydrogenation of Furfural. *ACS Sustain. Chem. Eng.* **2018**, *6*, 16235–16247. [CrossRef]

14. Wang, Y.; Zhao, D.; Rodríguez-Padrón, D.; Len, C. Recent Advances in Catalytic Hydrogenation of Furfural. *Catalysts* **2019**, *9*, 796. [CrossRef]
15. Pizzi, R.; van Putten, R.-J.; Brust, H.; Perathoner, S.; Centi, G.; van der Waal, J. High-Throughput Screening of Heterogeneous Catalysts for the Conversion of Furfural to Bio-Based Fuel Components. *Catalysts* **2015**, *5*, 2244–2257. [CrossRef]
16. Rodríguez-Machín, L.; Piloto-Rodríguez, R.; Rubio-González, A.; Iturria-Quintero, P.J.; Ronsse, F. Pretreatment of Sugarcane Residues for Combustion in Biomass Power Stations: A Review. *Sugar Tech* **2022**, *24*, 732–745. [CrossRef]
17. Borgogna, A.; Centi, G.; Iaquaniello, G.; Perathoner, S.; Papanikolaou, G.; Salladini, A. Assessment of Hydrogen Production from Municipal Solid Wastes as Competitive Route to Produce Low-Carbon H_2. *Sci. Total Environ.* **2022**, *827*, 154393. [CrossRef]
18. Catizzone, E.; Migliori, M.; Purita, A.; Giordano, G. Ferrierite vs. Γ-Al_2O_3: The Superiority of Zeolites in Terms of Water-Resistance in Vapour-Phase Dehydration of Methanol to Dimethyl Ether. *J. Energy Chem.* **2019**, *30*, 162–169. [CrossRef]
19. Migliori, M.; Aloise, A.; Catizzone, E.; Giordano, G. Kinetic Analysis of Methanol to Dimethyl Ether Reaction over H-MFI Catalyst. *Ind. Eng. Chem. Res.* **2014**, *53*, 14885–14891. [CrossRef]
20. Semelsberger, T.A.; Borup, R.L.; Greene, H.L. Dimethyl Ether (DME) as an Alternative Fuel. *J. Power Source* **2006**, *156*, 497–511. [CrossRef]
21. Catizzone, E.; Aloise, A.; Migliori, M.; Giordano, G. Dimethyl Ether Synthesis via Methanol Dehydration: Effect of Zeolite Structure. *Appl. Catal. A Gen.* **2015**, *502*, 215–220. [CrossRef]
22. Migliori, M.; Catizzone, E.; Aloise, A.; Bonura, G.; Gómez-Hortigüela, L.; Frusteri, L.; Cannilla, C.; Frusteri, F.; Giordano, G. New Insights about Coke Deposition in Methanol-to-DME Reaction over MOR-, MFI- and FER-Type Zeolites. *J. Ind. Eng. Chem.* **2018**, *68*, 196–208. [CrossRef]
23. Migliori, M.; Condello, A.; Dalena, F.; Catizzone, E.; Giordano, G. CuZnZr-Zeolite Hybrid Grains for DME Synthesis: New Evidence on the Role of Metal-Acidic Features on the Methanol Conversion Step. *Catalysts* **2020**, *10*, 671. [CrossRef]
24. Catizzone, E.; Giglio, E.; Migliori, M.; Cozzucoli, P.C.; Giordano, G. The Effect of Zeolite Features on the Dehydration Reaction of Methanol to Dimethyl Ether: Catalytic Behaviour and Kinetics. *Materials* **2020**, *13*, 5577. [CrossRef]
25. Jhang, S.; Lin, Y.-C.; Chen, K.; Lin, S.; Batterman, S. Evaluation of Fuel Consumption, Pollutant Emissions and Well-to-Wheel GHGs Assessment from a Vehicle Operation Fueled with Bioethanol, Gasoline and Hydrogen. *Energy* **2020**, *209*, 118436. [CrossRef]
26. Zabed, H.; Sahu, J.N.; Suely, A.; Boyce, A.N.; Faruq, G. Bioethanol Production from Renewable Sources: Current Perspectives and Technological Progress. *Renew. Sustain. Energy Rev.* **2017**, *71*, 475–501. [CrossRef]
27. Kadam, S.A.; Shamzhy, M.V. IR Operando Study of Ethanol Dehydration over MFI Zeolite. *Catal. Today* **2018**, *304*, 51–57. [CrossRef]
28. Tarach, K.A.; Tekla, J.; Filek, U.; Szymocha, A.; Tarach, I.; Góra-Marek, K. Alkaline-Acid Treated Zeolite L as Catalyst in Ethanol Dehydration Process. *Microporous Mesoporous Mater.* **2017**, *241*, 132–144. [CrossRef]
29. Phung, T.K.; Proietti Hernández, L.; Lagazzo, A.; Busca, G. Dehydration of Ethanol over Zeolites, Silica Alumina and Alumina: Lewis Acidity, Brønsted Acidity and Confinement Effects. *Appl. Catal. A Gen.* **2015**, *493*, 77–89. [CrossRef]
30. Zoppi, G.; Pipitone, G.; Pirone, R.; Bensaid, S. Aqueous Phase Reforming Process for the Valorization of Wastewater Streams: Application to Different Industrial Scenarios. *Catal. Today* **2022**, *387*, 224–236. [CrossRef]
31. Sharma, Y.C.; Kumar, A.; Prasad, R.; Upadhyay, S.N. Ethanol Steam Reforming for Hydrogen Production: Latest and Effective Catalyst Modification Strategies to Minimize Carbonaceous Deactivation. *Renew. Sustain. Energy Rev.* **2017**, *74*, 89–103. [CrossRef]
32. Ni, M.; Leung, D.Y.C.; Leung, M.K.H. A Review on Reforming Bio-Ethanol for Hydrogen Production. *Int. J. Hydrogen Energy* **2007**, *32*, 3238–3247. [CrossRef]
33. Ogo, S.; Sekine, Y. Recent Progress in Ethanol Steam Reforming Using Non-Noble Transition Metal Catalysts: A Review. *Fuel Process. Technol.* **2020**, *199*, 106238. [CrossRef]
34. Frusteri, F.; Freni, S.; Spadaro, L.; Chiodo, V.; Bonura, G.; Donato, S.; Cavallaro, S. H_2 Production for MC Fuel Cell by Steam Reforming of Ethanol over MgO Supported Pd, Rh, Ni and Co Catalysts. *Catal. Commun.* **2004**, *5*, 611–615. [CrossRef]
35. Wang, Z.; Zhang, X.; Rezazadeh, A. Hydrogen Fuel and Electricity Generation from a New Hybrid Energy System Based on Wind and Solar Energies and Alkaline Fuel Cell. *Energy Rep.* **2021**, *7*, 2594–2604. [CrossRef]
36. Khan, U.; Yamamoto, T.; Sato, H. An Insight into Potential Early Adopters of Hydrogen Fuel-Cell Vehicles in Japan. *Int. J. Hydrogen Energy* **2021**, *46*, 10589–10607. [CrossRef]
37. Eba, H.; Masuzoe, Y.; Sugihara, T.; Yagi, H.; Liu, T. Ammonia Production Using Iron Nitride and Water as Hydrogen Source under Mild Temperature and Pressure. *Int. J. Hydrogen Energy* **2021**, *46*, 10642–10652. [CrossRef]
38. Giglio, E.; Vitale, G.; Lanzini, A.; Santarelli, M. Integration between Biomass Gasification and High-Temperature Electrolysis for Synthetic Methane Production. *Biomass Bioenergy* **2021**, *148*, 106017. [CrossRef]
39. Giglio, E.; Pirone, R.; Bensaid, S. Dynamic Modelling of Methanation Reactors during Start-up and Regulation in Intermittent Power-to-Gas Applications. *Renew. Energy* **2021**, *170*, 1040–1051. [CrossRef]
40. Guzmán, H.; Salomone, F.; Bensaid, S.; Castellino, M.; Russo, N.; Hernández, S. CO_2 Conversion to Alcohols over Cu/ZnO Catalysts: Prospective Synergies between Electrocatalytic and Thermocatalytic Routes. *ACS Appl. Mater. Interfaces* **2022**, *14*, 517–530. [CrossRef] [PubMed]
41. Marchese, M.; Heikkinen, N.; Giglio, E.; Lanzini, A.; Lehtonen, J.; Reinikainen, M. Kinetic Study Based on the Carbide Mechanism of a Co-Pt/γ-Al_2O_3 Fischer–Tropsch Catalyst Tested in a Laboratory-Scale Tubular Reactor. *Catalysts* **2019**, *9*, 717. [CrossRef]

42. Pein, M.; Neumann, N.C.; Venstrom, L.J.; Vieten, J.; Roeb, M.; Sattler, C. Two-Step Thermochemical Electrolysis: An Approach for Green Hydrogen Production. *Int. J. Hydrogen Energy* **2021**, *46*, 24909–24918. [CrossRef]
43. Freire Ordóñez, D.; Shah, N.; Guillén-Gosálbez, G. Economic and Full Environmental Assessment of Electrofuels via Electrolysis and Co-Electrolysis Considering Externalities. *Appl. Energy* **2021**, *286*, 116488. [CrossRef]
44. Martinelli, M.; Castro, J.D.; Alhraki, N.; Matamoros, M.E.; Kropf, A.J.; Cronauer, D.C.; Jacobs, G. Effect of Sodium Loading on Pt/ZrO_2 during Ethanol Steam Reforming. *Appl. Catal. A Gen.* **2021**, *610*, 117947. [CrossRef]
45. Chen, W.-H.; Li, S.; Lim, S.; Chen, Z.; Juan, J.C. Reaction and Hydrogen Production Phenomena of Ethanol Steam Reforming in a Catalytic Membrane Reactor. *Energy* **2021**, *220*, 119737. [CrossRef]
46. Zhurka, M.D.; Lemonidou, A.A.; Anderson, J.A.; Kechagiopoulos, P.N. Kinetic Analysis of the Steam Reforming of Ethanol over Ni/SiO_2 for the Elucidation of Metal-Dominated Reaction Pathways. *React. Chem. Eng.* **2018**, *3*, 883–897. [CrossRef]
47. Grzybek, G.; Góra-Marek, K.; Patulski, P.; Greluk, M.; Rotko, M.; Słowik, G.; Kotarba, A. Optimization of the Potassium Promotion of the $Co/\alpha\text{-}Al_2O_3$ Catalyst for the Effective Hydrogen Production via Ethanol Steam Reforming. *Appl. Catal. A Gen.* **2021**, *614*, 118051. [CrossRef]
48. Ghasemzadeh, K.; Jalilnejad, E.; Sadati Tilebon, S.M. Hydrogen Production Technologies from Ethanol. In *Ethanol*; Elsevier: Amsterdam, The Netherlands, 2019; pp. 307–340, ISBN 9780128114582.
49. Li, M.-R.; Wang, G.-C. The Mechanism of Ethanol Steam Reforming on the Co^0 and Co^{2+} Sites: A DFT Study. *J. Catal.* **2018**, *365*, 391–404. [CrossRef]
50. Kumar, A.; Prasad, R.; Sharma, Y.C. Ethanol Steam Reforming Study over ZSM-5 Supported Cobalt versus Nickel Catalyst for Renewable Hydrogen Generation. *Chinese J. Chem. Eng.* **2019**, *27*, 677–684. [CrossRef]
51. Roychowdhury, S.; Mukthar Ali, M.; Dhua, S.; Sundararajan, T.; Ranga Rao, G. Thermochemical Hydrogen Production Using $Rh/CeO_2/\gamma\text{-}Al_2O_3$ Catalyst by Steam Reforming of Ethanol and Water Splitting in a Packed Bed Reactor. *Int. J. Hydrogen Energy* **2021**, *46*, 19254–19269. [CrossRef]
52. Martínez, A.H.; Lopez, E.; Cadús, L.E.; Agüero, F.N. Elucidation of the Role of Support in Rh/Perovskite Catalysts Used in Ethanol Steam Reforming Reaction. *Catal. Today* **2021**, *372*, 59–69. [CrossRef]
53. Greluk, M.; Rotko, M.; Słowik, G.; Turczyniak-Surdacka, S. Hydrogen Production by Steam Reforming of Ethanol over Co/CeO_2 Catalysts: Effect of Cobalt Content. *J. Energy Inst.* **2019**, *92*, 222–238. [CrossRef]
54. Nejat, T.; Jalalinezhad, P.; Hormozi, F.; Bahrami, Z. Hydrogen Production from Steam Reforming of Ethanol over Ni-Co Bimetallic Catalysts and MCM-41 as Support. *J. Taiwan Inst. Chem. Eng.* **2019**, *97*, 216–226. [CrossRef]
55. Ferencz, Z.; Varga, E.; Puskás, R.; Kónya, Z.; Baán, K.; Oszkó, A.; Erdőhelyi, A. Reforming of Ethanol on Co/Al_2O_3 Catalysts Reduced at Different Temperatures. *J. Catal.* **2018**, *358*, 118–130. [CrossRef]
56. Lang, L.; Zhao, S.; Yin, X.; Yang, W.; Wu, C. Catalytic Activities of K-Modified Zeolite ZSM-5 Supported Rhodium Catalysts in Low-Temperature Steam Reforming of Bioethanol. *Int. J. Hydrogen Energy* **2015**, *40*, 9924–9934. [CrossRef]
57. Vizcaino, A.; Carrero, A.; Calles, J. Hydrogen Production by Ethanol Steam Reforming over Cu–Ni Supported Catalysts. *Int. J. Hydrogen Energy* **2007**, *32*, 1450–1461. [CrossRef]
58. Phung, T.K.; Busca, G. Diethyl Ether Cracking and Ethanol Dehydration: Acid Catalysis and Reaction Paths. *Chem. Eng. J.* **2015**, *272*, 92–101. [CrossRef]
59. Rossetti, I.; Compagnoni, M.; Finocchio, E.; Ramis, G.; Di Michele, A.; Zucchini, A.; Dzwigaj, S. Syngas Production via Steam Reforming of Bioethanol over Ni–BEA Catalysts: A BTL Strategy. *Int. J. Hydrogen Energy* **2016**, *41*, 16878–16889. [CrossRef]
60. Anggoro, D.D.; Oktavianty, H.; Sasongko, S.B.; Buchori, L. Effect of Dealumination on the Acidity of Zeolite Y and the Yield of Glycerol Mono Stearate (GMS). *Chemosphere* **2020**, *257*, 127012. [CrossRef] [PubMed]
61. Dias, S.C.L.; Dias, J.A. Effects of the Dealumination Methodology on the FER Zeolite Acidity: A Study with Fractional Factorial Design. *Mol. Catal.* **2018**, *458*, 139–144. [CrossRef]
62. Peron, D.V.; Zholobenko, V.L.; de Melo, J.H.S.; Capron, M.; Nuns, N.; de Souza, M.O.; Feris, L.A.; Marcilio, N.R.; Ordomsky, V.V.; Khodakov, A.Y. External Surface Phenomena in Dealumination and Desilication of Large Single Crystals of ZSM-5 Zeolite Synthesized from a Sustainable Source. *Microporous Mesoporous Mater.* **2019**, *286*, 57–64. [CrossRef]
63. Li, D.; Li, X.; Gong, J. Catalytic Reforming of Oxygenates: State of the Art and Future Prospects. *Chem. Rev.* **2016**, *116*, 11529–11653. [CrossRef] [PubMed]
64. Contreras, J.L.; Salmones, J.; Colín-Luna, J.A.; Nuño, L.; Quintana, B.; Córdova, I.; Zeifert, B.; Tapia, C.; Fuentes, G.A. Catalysts for H_2 Production Using the Ethanol Steam Reforming (a Review). *Int. J. Hydrogen Energy* **2014**, *39*, 18835–18853. [CrossRef]
65. Zanchet, D.; Santos, J.B.O.; Damyanova, S.; Gallo, J.M.R.; Bueno, J.M.C. Toward Understanding Metal-Catalyzed Ethanol Reforming. *ACS Catal.* **2015**, *5*, 3841–3863. [CrossRef]
66. Choi, Y.; Liu, P. Understanding of Ethanol Decomposition on Rh(1 1 1) from Density Functional Theory and Kinetic Monte Carlo Simulations. *Catal. Today* **2011**, *165*, 64–70. [CrossRef]
67. Sutton, J.E.; Vlachos, D.G. Ethanol Activation on Closed-Packed Surfaces. *Ind. Eng. Chem. Res.* **2015**, *54*, 4213–4225. [CrossRef]
68. Jones, G.; Jakobsen, J.G.; Shim, S.S.; Kleis, J.; Andersson, M.P.; Rossmeisl, J.; Abild-Pedersen, F.; Bligaard, T.; Helveg, S.; Hinnemann, B.; et al. First Principles Calculations and Experimental Insight into Methane Steam Reforming over Transition Metal Catalysts. *J. Catal.* **2008**, *259*, 147–160. [CrossRef]

69. Wang, S.; He, B.; Tian, R.; Sun, C.; Dai, R.; Li, X.; Wu, X.; An, X.; Xie, X. Ni-Hierarchical Beta Zeolite Catalysts Were Applied to Ethanol Steam Reforming: Effect of Sol Gel Method on Loading Ni and the Role of Hierarchical Structure. *Mol. Catal.* **2018**, *453*, 64–73. [CrossRef]
70. Iulianelli, A.; Dalena, F.; Basile, A. Steam Reforming, Preferential Oxidation, and Autothermal Reforming of Ethanol for Hydrogen Production in Membrane Reactors. In *Ethanol*; Elsevier: Amsterdam, The Netherlands, 2019; pp. 193–213, ISBN 9780128114582.
71. Phung, T.K.; Pham, T.L.M.; Nguyen, A.-N.T.; Vu, K.B.; Giang, H.N.; Nguyen, T.; Huynh, T.C.; Pham, H.D. Effect of Supports and Promoters on the Performance of Ni-Based Catalysts in Ethanol Steam Reforming. *Chem. Eng. Technol.* **2020**, *43*, 672–688. [CrossRef]
72. Zheng, Z.; Sun, C.; Dai, R.; Wang, S.; Wu, X.; An, X.; Wu, Z.; Xie, X. Ethanol Steam Reforming on Ni-Based Catalysts: Effect of Cu and Fe Addition on the Catalytic Activity and Resistance to Deactivation. *Energy Fuels* **2017**, *31*, 3091–3100. [CrossRef]
73. Vicente, J.; Ereña, J.; Montero, C.; Azkoiti, M.J.; Bilbao, J.; Gayubo, A.G. Reaction Pathway for Ethanol Steam Reforming on a Ni/SiO_2 Catalyst Including Coke Formation. *Int. J. Hydrogen Energy* **2014**, *39*, 18820–18834. [CrossRef]
74. Kwak, B.S.; Lee, G.; Park, S.M.; Kang, M. Effect of MnOx in the Catalytic Stabilization of Co_2MnO_4 Spinel during the Ethanol Steam Reforming Reaction. *Appl. Catal. A Gen.* **2015**, *503*, 165–175. [CrossRef]
75. Greluk, M.; Gac, W.; Rotko, M.; Słowik, G.; Turczyniak-Surdacka, S. Co/CeO_2 and Ni/CeO_2 Catalysts for Ethanol Steam Reforming: Effect of the Cobalt/Nickel Dispersion on Catalysts Properties. *J. Catal.* **2021**, *393*, 159–178. [CrossRef]
76. Zhang, H.; Fan, Y.F.; Huan, Y.H.; Yue, M.B. Dry-Gel Synthesis of Shaped Transition-Metal-Doped M-MFI (M = Ti, Fe, Cr, Ni) Zeolites by Using Metal-Occluded Zeolite Seed Sol as a Directing Agent. *Microporous Mesoporous Mater.* **2016**, *231*, 178–185. [CrossRef]
77. Inokawa, H.; Maeda, M.; Nishimoto, S. Synthesis of Nickel Nanoparticles with Excellent Thermal Stability in Micropores of Zeolite. *Int. J. Hydrogen Energy* **2013**, *38*, 13579–13586. [CrossRef]
78. Bozbag, S.E.; Zhang, L.C.; Aindow, M.; Erkey, C. Carbon Aerogel Supported Nickel Nanoparticles and Nanorods Using Supercritical Deposition. *J. Supercrit. Fluids* **2012**, *66*, 265–273. [CrossRef]
79. Isarapakdeetham, S.; Kim-Lohsoontorn, P.; Wongsakulphasatch, S.; Kiatkittipong, W.; Laosiripojana, N.; Gong, J.; Assabumrungrat, S. Hydrogen Production via Chemical Looping Steam Reforming of Ethanol by Ni-Based Oxygen Carriers Supported on CeO_2 and La_2O_3 Promoted Al_2O_3. *Int. J. Hydrogen Energy* **2020**, *45*, 1477–1491. [CrossRef]
80. Zhang, L.; Liu, J.; Li, W. Ethanol Steam Reforming over $Ni-Cu/Al_2O_3-M_yO_z$ (M = Si, La, Mg, and Zn) Catalysts. *J. Nat. Gas Chem.* **2009**, *18*, 55–65. [CrossRef]
81. Zhurka, M.D.; Lemonidou, A.A.; Kechagiopoulos, P.N. Elucidation of Metal and Support Effects during Ethanol Steam Reforming over Ni and Rh Based Catalysts Supported on $(CeO_2)-ZrO_2-La_2O_3$. *Catal. Today* **2021**, *368*, 161–172. [CrossRef]
82. Garbarino, G.; Wang, C.; Valsamakis, I.; Chitsazan, S.; Riani, P.; Finocchio, E.; Flytzani-Stephanopoulos, M.; Busca, G. A Study of Ni/Al_2O_3 and $Ni–La/Al_2O_3$ Catalysts for the Steam Reforming of Ethanol and Phenol. *Appl. Catal. B Environ.* **2015**, *174–175*, 21–34. [CrossRef]
83. Song, J.H.; Yoo, S.; Yoo, J.; Park, S.; Gim, M.Y.; Kim, T.H.; Song, I.K. Hydrogen Production by Steam Reforming of Ethanol over $Ni/Al_2O_3-La_2O_3$ Xerogel Catalysts. *Mol. Catal.* **2017**, *434*, 123–133. [CrossRef]
84. Campos-Skrobot, F.C.; Rizzo-Domingues, R.C.P.; Fernandes-Machado, N.R.C.; Cantão, M.P. Novel Zeolite-Supported Rhodium Catalysts for Ethanol Steam Reforming. *J. Power Source* **2008**, *183*, 713–716. [CrossRef]
85. Gac, W.; Greluk, M.; Słowik, G.; Millot, Y.; Valentin, L.; Dzwigaj, S. Effects of Dealumination on the Performance of Ni-Containing BEA Catalysts in Bioethanol Steam Reforming. *Appl. Catal. B Environ.* **2018**, *237*, 94–109. [CrossRef]
86. Bizkarra, K.; Barrio, V.L.; Gartzia-Rivero, L.; Bañuelos, J.; López-Arbeloa, I.; Cambra, J.F. Hydrogen Production from a Model Bio-Oil/Bio-Glycerol Mixture through Steam Reforming Using Zeolite L Supported Catalysts. *Int. J. Hydrogen Energy* **2019**, *44*, 1492–1504. [CrossRef]
87. Rodriguez-Gomez, A.; Caballero, A. Bimetallic Ni-Co/SBA-15 Catalysts for Reforming of Ethanol: How Cobalt Modifies the Nickel Metal Phase and Product Distribution. *Mol. Catal.* **2018**, *449*, 122–130. [CrossRef]
88. Lindo, M.; Vizcaíno, A.J.; Calles, J.A.; Carrero, A. Ethanol Steam Reforming on Ni/Al-SBA-15 Catalysts: Effect of the Aluminium Content. *Int. J. Hydrogen Energy* **2010**, *35*, 5895–5901. [CrossRef]
89. Bayram, B.; Soykal, I.I.; Von Deak, D.; Miller, J.T.; Ozkan, U.S. Ethanol Steam Reforming over Co-Based Catalysts: Investigation of Cobalt Coordination Environment under Reaction Conditions. *J. Catal.* **2011**, *284*, 77–89. [CrossRef]
90. Garbarino, G.; Cavattoni, T.; Riani, P.; Brescia, R.; Canepa, F.; Busca, G. On the Role of Support in Metallic Heterogeneous Catalysis: A Study of Unsupported Nickel–Cobalt Alloy Nanoparticles in Ethanol Steam Reforming. *Catal. Lett.* **2019**, *149*, 929–941. [CrossRef]
91. Pinton, N.; Vidal, M.V.; Signoretto, M.; Martínez-Arias, A.; Cortés Corberán, V. Ethanol Steam Reforming on Nanostructured Catalysts of Ni, Co and CeO_2: Influence of Synthesis Method on Activity, Deactivation and Regenerability. *Catal. Today* **2017**, *296*, 135–143. [CrossRef]
92. Rodriguez-Gomez, A.; Holgado, J.P.; Caballero, A. Cobalt Carbide Identified as Catalytic Site for the Dehydrogenation of Ethanol to Acetaldehyde. *ACS Catal.* **2017**, *7*, 5243–5247. [CrossRef]
93. Gonçalves, A.A.S.; Faustino, P.B.; Assaf, J.M.; Jaroniec, M. One-Pot Synthesis of Mesoporous Ni-Ti-Al Ternary Oxides: Highly Active and Selective Catalysts for Steam Reforming of Ethanol. *ACS Appl. Mater. Interfaces* **2017**, *9*, 6079–6092. [CrossRef]

94. Słowik, G.; Greluk, M.; Rotko, M.; Machocki, A. Evolution of the Structure of Unpromoted and Potassium-Promoted Ceria-Supported Nickel Catalysts in the Steam Reforming of Ethanol. *Appl. Catal. B Environ.* **2018**, *221*, 490–509. [CrossRef]
95. Riani, P.; Garbarino, G.; Canepa, F.; Busca, G. Cobalt Nanoparticles Mechanically Deposited on α-Al_2O_3: A Competitive Catalyst for the Production of Hydrogen through Ethanol Steam Reforming. *J. Chem. Technol. Biotechnol.* **2019**, *94*, 538–546. [CrossRef]
96. Chen, M.; Wang, C.; Wang, Y.; Tang, Z.; Yang, Z.; Zhang, H.; Wang, J. Hydrogen Production from Ethanol Steam Reforming: Effect of Ce Content on Catalytic Performance of Co/Sepiolite Catalyst. *Fuel* **2019**, *247*, 344–355. [CrossRef]
97. Parlett, C.M.A.; Aydin, A.; Durndell, L.J.; Frattini, L.; Isaacs, M.A.; Lee, A.F.; Liu, X.; Olivi, L.; Trofimovaite, R.; Wilson, K.; et al. Tailored Mesoporous Silica Supports for Ni Catalysed Hydrogen Production from Ethanol Steam Reforming. *Catal. Commun.* **2017**, *91*, 76–79. [CrossRef]
98. da Silva, A.L.M.; den Breejen, J.P.; Mattos, L.V.; Bitter, J.H.; de Jong, K.P.; Noronha, F.B. Cobalt Particle Size Effects on Catalytic Performance for Ethanol Steam Reforming – Smaller Is Better. *J. Catal.* **2014**, *318*, 67–74. [CrossRef]
99. Kourtelesis, M.; Verykios, X. Stability of Pt/γ-Al_2O_3 Catalyst for the Low Temperature Steam Reforming of Ethanol & Acetaldehyde. Effect of Carrier Modification with Ca. *Mater. Today Proc.* **2018**, *5*, 27406–27415. [CrossRef]
100. Wu, Y.; Chung, W.; Chang, M. Modification of Ni/γ-Al_2O_3 Catalyst with Plasma for Steam Reforming of Ethanol to Generate Hydrogen. *Int. J. Hydrogen Energy* **2015**, *40*, 8071–8080. [CrossRef]
101. Lucredio, A.F.; Bellido, J.D.A.; Zawadzki, A.; Assaf, E.M. Co Catalysts Supported on SiO_2 and γ-Al_2O_3 Applied to Ethanol Steam Reforming: Effect of the Solvent Used in the Catalyst Preparation Method. *Fuel* **2011**, *90*, 1424–1430. [CrossRef]
102. Kim, D.; Sub, B.; Min, B.; Kang, M. Applied Surface Science Characterization of Ni and W Co-Loaded SBA-15 Catalyst and Its Hydrogen Production Catalytic Ability on Ethanol Steam Reforming Reaction. *Appl. Surf. Sci.* **2015**, *332*, 736–746. [CrossRef]
103. He, S.; He, S.; Zhang, L.; Li, X.; Wang, J.; He, D.; Lu, J.; Luo, Y. Hydrogen Production by Ethanol Steam Reforming over Ni/SBA-15 Mesoporous Catalysts: Effect of Au Addition. *Catal. Today* **2015**, *258*, 162–168. [CrossRef]
104. Bussi, J.; Musso, M.; Veiga, S.; Bespalko, N.; Faccio, R.; Roger, A. Ethanol Steam Reforming over NiLaZr and NiCuLaZr Mixed Metal Oxide Catalysts. *Catal. Today* **2013**, *213*, 42–49. [CrossRef]
105. Coleman, L.J.I.; Epling, W.; Hudgins, R.R.; Croiset, E. Ni/Mg–Al Mixed Oxide Catalyst for the Steam Reforming of Ethanol. *Appl. Catal. A Gen.* **2009**, *363*, 52–63. [CrossRef]
106. Marino, A.; Aloise, A.; Hernando, H.; Fermoso, J.; Cozza, D.; Giglio, E.; Migliori, M.; Pizarro, P.; Giordano, G.; Serrano, D.P. ZSM-5 Zeolites Performance Assessment in Catalytic Pyrolysis of PVC-Containing Real WEEE Plastic Wastes. *Catal. Today* **2022**, *390–391*, 210–220. [CrossRef]
107. Cychosz, K.A.; Guillet-Nicolas, R.; García-Martínez, J.; Thommes, M. Recent Advances in the Textural Characterization of Hierarchically Structured Nanoporous Materials. *Chem. Soc. Rev.* **2017**, *46*, 389–414. [CrossRef] [PubMed]
108. Centi, G.; Perathoner, S.; Pino, F.; Arrigo, R.; Giordano, G.; Katovic, A.; Pedulà, V. Performances of Fe-[Al, B]MFI Catalysts in Benzene Hydroxylation with N_2O: The Role of Zeolite Defects as Host Sites for Highly Active Iron Species. *Catal. Today* **2005**, *110*, 211–220. [CrossRef]
109. Katovic, A.; Giordano, G.; Bonelli, B.; Onida, B.; Garrone, E.; Lentz, P.; Nagy, J.B. Preparation and Characterization of Mesoporous Molecular Sieves Containing Al, Fe or Zn. *Microporous Mesoporous Mater.* **2001**, *44–45*, 275–281. [CrossRef]
110. Sandoval-Díaz, L.-E.; González-Amaya, J.-A.; Trujillo, C.-A. General Aspects of Zeolite Acidity Characterization. *Microporous Mesoporous Mater.* **2015**, *215*, 229–243. [CrossRef]
111. Weitkamp, J. Zeolites and Catalysis. *Solid State Ionics* **2000**, *131*, 175–188. [CrossRef]
112. Maesen, T. The Zeolite Scene—An Overview. In *Introduction to Zeolite Science and Practice*; Čejka, J., van Bekkum, H., Corma, A., Schüth, F., Eds.; Elsevier: Amsterdam, The Netherlands, 2007; Volume 168, pp. 1–12, ISBN 0444530630.
113. Milliken, T.H.; Mills, G.A.; Oblad, A.G. The Chemical Characteristics and Structure of Cracking Catalysts. *Discuss. Faraday Soc.* **1950**, *8*, 279–290. [CrossRef]
114. Busca, G. Acidity and Basicity of Zeolites: A Fundamental Approach. *Microporous Mesoporous Mater.* **2017**, *254*, 3–16. [CrossRef]
115. Madeira, F.F.; Gnep, N.S.; Magnoux, P.; Maury, S.; Cadran, N. Ethanol Transformation over HFAU, HBEA and HMFI Zeolites Presenting Similar Brønsted Acidity. *Appl. Catal. A Gen.* **2009**, *367*, 39–46. [CrossRef]
116. Santi, D.; Rabl, S.; Calemma, V.; Dyballa, M.; Hunger, M.; Weitkamp, J. Effect of Noble Metals on the Strength of Brønsted Acid Sites in Bifunctional Zeolites. *ChemCatChem* **2013**, *5*, 1524–1530. [CrossRef]
117. Aloise, A.; Marino, A.; Dalena, F.; Giorgianni, G.; Migliori, M.; Frusteri, L.; Cannilla, C.; Bonura, G.; Frusteri, F.; Giordano, G. Desilicated ZSM-5 Zeolite: Catalytic Performances Assessment in Methanol to DME Dehydration. *Microporous Mesoporous Mater.* **2020**, *302*, 110198. [CrossRef]
118. Dalena, F.; Giglio, E.; Giorgianni, G.; Cozza, D.; Marino, A.; Aloise, A. DME Production via Methanol Dehydration with H Form and Desilicated ZSM-5 Type Zeolitic Catalysts: Study on the Correlation between Acid Sites and Conversion. *Chem. Eng. Trans.* **2021**, *84*, 211–216. [CrossRef]
119. Rossetti, I.; Lasso, J.; Nichele, V.; Signoretto, M.; Finocchio, E.; Ramis, G.; Di Michele, A. Silica and Zirconia Supported Catalysts for the Low-Temperature Ethanol Steam Reforming. *Appl. Catal. B Environ.* **2014**, *150–151*, 257–267. [CrossRef]
120. Gołąbek, K.; Tarach, K.A.; Filek, U.; Góra-Marek, K. Ethylene Formation by Dehydration of Ethanol over Medium Pore Zeolites. *Spectrochim. Acta Part A Mol. Biomol. Spectrosc.* **2018**, *192*, 464–472. [CrossRef]
121. Kuz'mina, R.I.; Frolov, M.P.; Liventsev, V.T.; Vetrova, T.K.; Kovnev, A. V Development of Zeolite-Containing Reforming Catalysts. *Catal. Ind.* **2010**, *2*, 329–333. [CrossRef]

122. Čejka, J.; van Bekkum, H.; Corma, A.; Schüth, F. (Eds.) *Introduction to Zeolite Science and Practice*, 3rd ed.; Elsevier B.V.: Amsterdam, The Netherlands, 2007.
123. Da Costa-Serra, J.F.; Navarro, M.T.; Rey, F.; Chica, A. Bioethanol Steam Reforming on Ni-Based Modified Mordenite. Effect of Mesoporosity, Acid Sites and Alkaline Metals. *Int. J. Hydrogen Energy* **2012**, *37*, 7101–7108. [CrossRef]
124. Rokicińska, A.; Drozdek, M.; Dudek, B.; Gil, B.; Michorczyk, P.; Brouri, D.; Dzwigaj, S.; Kuśtrowski, P. Cobalt-Containing BEA Zeolite for Catalytic Combustion of Toluene. *Appl. Catal. B Environ.* **2017**, *212*, 59–67. [CrossRef]
125. Newsam, J.M.; Treacy, M.M.J.; Koetsier, W.T.; De Gruyter, C.B. Structural Characterization of Zeolite Beta. *Proc. R. Soc. Lond. A. Math. Phys. Sci.* **1988**, *420*, 375–405. [CrossRef]
126. International Zeolite Association (IZA)—Database of Zeolite Structures. Available online: http://www.iza-structure.org/databases/ (accessed on 28 April 2022).
127. Pinheiro, A.N.; Valentini, A.; Sasaki, J.M.; Oliveira, A.C. Highly Stable Dealuminated Zeolite Support for the Production of Hydrogen by Dry Reforming of Methane. *Appl. Catal. A Gen.* **2009**, *355*, 156–168. [CrossRef]
128. Che, Q.; Yang, M.; Wang, X.; Yang, Q.; Rose Williams, L.; Yang, H.; Zou, J.; Zeng, K.; Zhu, Y.; Chen, Y.; et al. Influence of Physicochemical Properties of Metal Modified ZSM-5 Catalyst on Benzene, Toluene and Xylene Production from Biomass Catalytic Pyrolysis. *Bioresour. Technol.* **2019**, *278*, 248–254. [CrossRef]
129. Shi, W.; Yi, B.; Hou, M.; Shao, Z. The Effect of H_2S and CO Mixtures on PEMFC Performance. *Int. J. Hydrogen Energy* **2007**, *32*, 4412–4417. [CrossRef]
130. Baschuk, J.J.; Li, X. Carbon Monoxide Poisoning of Proton Exchange Membrane Fuel Cells. *Int. J. Energy Res.* **2001**, *25*, 695–713. [CrossRef]
131. Tian, R.; Wang, S.; Lian, C.; Wu, X.; An, X.; Xie, X. Synthesis of the Hierarchical Fe-Substituted Porous HBeta Zeolite and the Exploration of Its Catalytic Performance. *J. Fuel Chem. Technol.* **2019**, *47*, 1476–1485. [CrossRef]
132. Centi, G.; Perathoner, S.; Arrigo, R.; Giordano, G.; Katovic, A.; Pedulà, V. Characterization and Reactivity of Fe-[Al,B]MFI Catalysts for Benzene Hydroxylation with N_2O. *Appl. Catal. A Gen.* **2006**, *307*, 30–41. [CrossRef]
133. Centi, G.; Genovese, C.; Giordano, G.; Katovic, A.; Perathoner, S. Performance of Fe–BEA Catalysts for the Selective Hydroxylation of Benzene with N_2O. *Catal. Today* **2004**, *91–92*, 17–26. [CrossRef]
134. Zheng, Z.; Sun, C.; Dai, R.; Wang, S.; Wu, X.; An, X.; Xie, X. Organotemplate-Free Synthesis of Hollow Beta Zeolite Supported Pt-Based Catalysts for Low-Temperature Ethanol Steam Reforming. *Catal. Sci. Technol.* **2016**, *6*, 6472–6475. [CrossRef]
135. Khaleque, A.; Alam, M.M.; Hoque, M.; Mondal, S.; Haider, J.B.; Xu, B.; Johir, M.A.H.; Karmakar, A.K.; Zhou, J.L.; Ahmed, M.B.; et al. Zeolite Synthesis from Low-Cost Materials and Environmental Applications: A Review. *Environ. Adv.* **2020**, *2*, 100019. [CrossRef]
136. Lutz, W. Zeolite Y: Synthesis, Modification, and Properties—A Case Revisited. *Adv. Mater. Sci. Eng.* **2014**, *2014*, 1–20. [CrossRef]
137. Sang, S.; Liu, Z.; Tian, P.; Liu, Z.; Qu, L.; Zhang, Y. Synthesis of Small Crystals Zeolite NaY. *Mater. Lett.* **2006**, *60*, 1131–1133. [CrossRef]
138. Domoroshchina, E.N.; Chernyshev, V.V.; Kuz'micheva, G.M.; Dorokhov, A.V.; Pirutko, L.V.; Kravchenko, G.V.; Chumakov, R.B. Changing the Characteristics and Properties of Zeolite Y and Nano-Anatase in the Formation of a Nano-Anatase/Y Composite with Improved Photocatalytic and Adsorption Properties. *Appl. Nanosci.* **2018**, *8*, 19–31. [CrossRef]
139. Inokawa, H.; Nishimoto, S.; Kameshima, Y.; Miyake, M. Difference in the Catalytic Activity of Transition Metals and Their Cations Loaded in Zeolite Y for Ethanol Steam Reforming. *Int. J. Hydrogen Energy* **2010**, *35*, 11719–11724. [CrossRef]
140. Inokawa, H.; Nishimoto, S.; Kameshima, Y.; Miyake, M. Promotion of H_2 Production from Ethanol Steam Reforming by Zeolite Basicity. *Int. J. Hydrogen Energy* **2011**, *36*, 15195–15202. [CrossRef]
141. Sub, B.; Su, J.; Sung, J.; Choi, B.; Jung, M.; Kang, M. Hydrogen-Rich Gas Production from Ethanol Steam Reforming over Ni/Ga/Mg/Zeolite Y Catalysts at Mild Temperature. *Appl. Energy* **2011**, *88*, 4366–4375. [CrossRef]
142. Chica, A.; Sayas, S. Effective and Stable Bioethanol Steam Reforming Catalyst Based on Ni and Co Supported on All-Silica Delaminated ITQ-2 Zeolite. *Catal. Today* **2009**, *146*, 37–43. [CrossRef]
143. Da Costa-Serra, J.F.; Chica, A. Bioethanol Steam Reforming on Co/ITQ-18 Catalyst: Effect of the Crystalline Structure of the Delaminated Zeolite ITQ-18. *Int. J. Hydrogen Energy* **2011**, *36*, 3862–3869. [CrossRef]
144. Giordano, G.; Migliori, M.; Ferrarelli, G.; Giorgianni, G.; Dalena, F.; Peng, P.; Debost, M.; Boullay, P.; Liu, Z.; Guo, H.; et al. Passivated Surface of High Aluminum Containing ZSM-5 by Silicalite-1: Synthesis and Application in Dehydration Reaction. *ACS Sustain. Chem. Eng.* **2022**, *10*, 4839–4848. [CrossRef]
145. Ferrarelli, G.; Giordano, G.; Migliori, M. ZSM-5@Sil-1 Core Shell: Effect of Synthesis Method over Textural and Catalytic Properties. *Catal. Today* **2022**, *390–391*, 176–184. [CrossRef]
146. Deng, Y.; Zhou, W.; Lv, H.; Zhang, Y.; Au, C.; Yin, S. Synthesis of HZSM-5@silicalite-1 Core–Shell Composite and Its Catalytic Application in the Generation of p-Xylene by Methylation of Toluene with Methyl Bromide. *RSC Adv.* **2014**, *4*, 37296–37301. [CrossRef]
147. Li, N.; Zhang, Y.; Chen, L.; Au, C.; Yin, S. Synthesis and Application of HZSM-5@silicalite-1 Core–Shell Composites for the Generation of Light Olefins from CH_3Br. *Microporous Mesoporous Mater.* **2016**, *227*, 76–80. [CrossRef]
148. Li, X.; Zheng, Z.; Wang, S.; Sun, C.; Dai, R.; Wu, X.; An, X.; Xie, X. Preparation and Characterization of Core–Shell Composite Zeolite BEA@MFI and Their Catalytic Properties in ESR. *Catal. Lett.* **2019**, *149*, 766–777. [CrossRef]

149. Bouizi, Y.; Diaz, I.; Rouleau, L.; Valtchev, V.P. Core-Shell Zeolite Microcomposites. *Adv. Funct. Mater.* **2005**, *15*, 1955–1960. [CrossRef]
150. Kwak, B.S.; Kim, J.; Kang, M. Hydrogen Production from Ethanol Steam Reforming over Core–Shell Structured Ni_xO_y–, Fe_xO_y–, and Co_xO_y–Pd Catalysts. *Int. J. Hydrogen Energy* **2010**, *35*, 11829–11843. [CrossRef]
151. Dai, R.; Zheng, Z.; Sun, C.; Li, X.; Wang, S.; Wu, X.; An, X.; Xie, X. Pt Nanoparticles Encapsulated in a Hollow Zeolite Microreactor as a Highly Active and Stable Catalyst for Low-Temperature Ethanol Steam Reforming. *Fuel* **2018**, *214*, 88–97. [CrossRef]
152. Zheng, Z.; Yang, D.; Li, T.; Yin, X.; Wang, S.; Wu, X.; An, X.; Xie, X. A Novel BEA-Type Zeolite Core–Shell Multiple Catalyst for Hydrogen-Rich Gas Production from Ethanol Steam Reforming. *Catal. Sci. Technol.* **2016**, *6*, 5427–5439. [CrossRef]
153. Wang, S.; He, B.; Tian, R.; Wu, X.; An, X.; Liu, Y.; Su, J.; Yu, Z.; Xie, X. Novel Core-Shell-like Ni-Supported Hierarchical Beta Zeolite Catalysts on Bioethanol Steam Reforming. *Int. J. Hydrogen Energy* **2020**, *45*, 16409–16420. [CrossRef]
154. Sun, C.; Zheng, Z.; Wang, S.; Li, X.; Wu, X.; An, X.; Xie, X. Yolk-Shell Structured Pt-CeO_2@Ni-SiO_2 as an Efficient Catalyst for Enhanced Hydrogen Production from Ethanol Steam Reforming. *Ceram. Int.* **2018**, *44*, 1438–1442. [CrossRef]
155. Pizzolitto, C.; Menegazzo, F.; Ghedini, E.; Innocenti, G.; Di Michele, A.; Cruciani, G.; Cavani, F.; Signoretto, M. Increase of Ceria Redox Ability by Lanthanum Addition on Ni Based Catalysts for Hydrogen Production. *ACS Sustain. Chem. Eng.* **2018**, *6*, 13867–13876. [CrossRef]
156. Dai, R.; Zheng, Z.; Shi, K.; Wu, X.; An, X.; Xie, X. A Multifunctional Core–Shell Nanoreactor with Unique Features of Sintering Resistance for High-Performance Ethanol Steam Reforming Reaction. *Fuel* **2021**, *287*, 119514. [CrossRef]